

Electronic Raman scattering in high-temperature superconductors

O V Misochko

DOI: 10.1070/PU2003v046n04ABEH001257

Contents

1. Introduction	373
2. Historical survey	374
3. Theoretical fundamentals of inelastic light scattering in a normal metal and in a superconductor	375
4. Experimental details	377
5. Experimental results and discussion	378
5.1 Electronic Raman spectra at optimal doping; 5.2 Light scattering with out-of-plane zz - and zx -polarizations;	
5.3 Light scattering in HTSC's with different doping levels; 5.4 Van Hove singularity and inelastic light scattering	
6. Symmetry of the order parameter, pairing, and possible superconductivity mechanisms	389
7. Conclusions	390
References	390

Abstract. Experimental results on, and theoretical fundamentals of, the electronic Raman scattering in high-temperature superconductors are discussed. The effects of temperature, impurity scattering, and resonance conditions on electronic Raman spectra in the superconducting state are analyzed. The primary objective of the review is to establish how different peculiarities of the inelastic light scattering spectra are related to fundamental properties of the fundamental superconducting state, such as the superconducting gap and the symmetry of pairing.

1. Introduction

At the end of 1986, Bednorz and Müller discovered superconductivity in the complex oxide La–Ba–Cu–O [1], and the exceptionally high temperature of the superconducting transition was the reason the new class of substances became known as high-temperature superconductors (HTSC's). This discovery, for which the two researchers were awarded the Nobel prize in 1987, set the task of establishing the mechanism of high-temperature superconductivity, which stimulated unprecedentedly high scientific activity and thus facilitated the development of many areas of physics. One such area was inelastic light scattering which is often called 'Raman scattering', but in Russian science literature known as 'combinational scattering of light'. The interest in Raman scattering is large because this phenomenon may be used to facilitate establishing the nature of high-temperature superconductivity, since it provides information about the symmetry of the superconducting order parameter.

The order parameter is a very convenient characteristic for describing the ordered states that emerge as a result of various phase transitions. The superconducting order parameter was introduced by Ginzburg and Landau in their phenomenological description of superconductivity [2]. It is a complex-valued function of coordinates, $\Psi(r)$, acting as a certain effective wave function that can be normalized so that $|\Psi(r)|^2$ is the density of the superconducting electrons. The relationship between the Ginzburg–Landau theory and the microscopic theory of Bardeen, Cooper, and Schrieffer (the BCS theory) was established by Gor'kov [3], and the order parameter $\Psi(r)$ was identified as the wave function of the ensemble of Cooper pairs, since it proved to be proportional to the energy gap $\Delta(r)$ in the spectrum of paired current carriers. The concept of electron pairing in the superconducting state [4, 5] remains valid for HTSC's. Indeed, the existence of Cooper pairs was convincingly demonstrated in early experiments on quantum flux quantization in a ring from polycrystalline $\text{YBa}_2\text{Cu}_3\text{O}_{7-x}$ (Y123) [6]. It is this pairing that leads to a specific response in the inelastic scattering of light by electrons [7], whose presence, combined with the possibility of probing the different regions of the Fermi surface within the given method, makes it possible to study the symmetry of the order parameter and to draw certain conclusions about the type of pairing [8].

A necessary condition for superconductivity is the emergence of off-diagonal long-range order [9]. Long-range order in a superconductor is caused by the anomalous nonvanishing average amplitude of a pair, and this anomalous average is simply the order parameter defined in the Ginzburg–Landau formalism [10]. In the momentum representation this order corresponds to the nonzero average $\langle c_{k\uparrow}c_{-k\downarrow} \rangle = -\langle c_{k\uparrow}^+c_{-k\downarrow}^+ \rangle \propto \Psi(k)$, where the wave function of the electron pair depends on the wave vector and is related to the gap function by the formula $\Psi(k) = \Delta_k/2E_k$, where E_k is the quasiparticle energy. The emergence of long-range order is accompanied by a lowering of symmetry, and, as in any second-order phase transition, the symmetries of the normal and superconducting states are interrelated, since

O V Misochko Institute of Solid State Physics,
Russian Academy of Sciences,
142432 Chernogolovka, Moscow Region, Russian Federation
Tel. (7-095) 993 27 55. Fax (7-096) 524 97 01
E-mail: misochko@issp.ac.ru

Received 23 May 2002

Uspekhi Fizicheskikh Nauk 173 (4) 385–405 (2003)

Translated by E Yankovsky; edited by M V Magnitskaya

the symmetry breaking in a superconducting transition is continuous [11]. Here the order parameter is simply the measure of symmetry breaking in the superconducting (ordered) state. The symmetry of the superconducting state must be the subgroup of the full symmetry group describing the normal state. This full symmetry group contains the symmetry groups of the crystal lattice, spin rotations, time reversal, and gauge. A transition to the superconducting state is always associated with a breakdown in gauge invariance [12]. If, in addition, we have a breakdown of one or more symmetries, a nontrivial order parameter is realized, and the gap function may have zeros in some regions of the reciprocal space [13]. A preliminary understanding of the symmetry of the HTSC order parameter can be gained from the group-theoretical approach. Since the crystal structures of all HTSC's have an inversion center, parity is a well-defined quantum number. This makes it possible to define the order parameter (the gap function) as a spin-triplet or spin-singlet state. Since the Josephson effect between superconductors of different parities disappears and the existing experimental data irrevocably prove that there is tunneling between HTSC's and classic elemental superconductors (such as Nb and Pb) [14, 15], we can limit ourselves to considering only singlet superconductivity. The next step requires examining the symmetry of the crystal lattice, since, according to Landau's theory, the order parameter must transform by one of the irreducible representations of the symmetry group of the high-temperature phase [10, 16]. Since HTSC's crystallize in orthorhombic or tetragonal structures [17], one is forced to consider the D_{2h} and D_{4h} groups (because superconductivity is realized in two-dimensional CuO_2 planes, often the two-dimensional subgroups C_{2v} and C_{4v} are considered instead of three-dimensional groups D_{2h} and D_{4h}). Table 1 lists the symmetries of the states that may be responsible for pairing in HTSC's [15].

The symmetry of the gap function can be determined through experiments even without knowing the microscopic mechanism of pairing, and recently many methods that make it possible to determine this symmetry have been realized [19]. The first group of such methods, which includes various interference measurements of the Josephson current, is

Table 1. Symmetry of the states of the tetragonal and orthorhombic groups.

Wave function	Irreducible representation	Basis function	Zeros
Point group D_{4h}			
s	A_{1g}	$1, x^2 + y^2, z^2$	no zeros
g	A_{2g}	$xy(x^2 - y^2)$	lines
$d_{x^2-y^2}$	B_{1g}	$x^2 - y^2$	lines
d_{xy}	B_{2g}	xy	lines
$e_{1,0}$	$E_g(1, 0)$	xz	lines
$e_{1,1}$	$E_g(1, 1)$	$(x + y)z$	lines
$e_{1,i}$	$E_g(1, i)$	$(x + iy)z$	lines
Point group D_{2h}			
s	A_g	$1, x^2, y^2, z^2$	no zeros
d_{xy}	B_{1g}	xy	lines
d_{xz}	B_{2g}	xz	lines
d_{yz}	B_{3g}	yz	lines

related to measuring the phase [15]. The second group is based on studying the thermodynamic properties. The third (and last) group incorporates spectroscopic measurements that probe the gap in the spectrum of the superconducting quasiparticles. The study of excitations of the superconducting state requires high resolution both in energy and in quasimomentum. In principle, neutron spectroscopy [20] satisfies both requirements, but several factors, such as available dimensions of single crystals and indirect, i.e., through the electron spin, interaction, limit the possibilities of neutron studies of the dynamics of the carriers. Angle-resolved photoemission is free of these limitations and, therefore, is used to establish the shape of the Fermi surface and to find the dependence of the superconducting gap Δ on the wave vector \mathbf{k} [21, 22]. Despite the high resolution in the quasimomentum \mathbf{k} , the energy resolution of photoemission is clearly insufficient for the detailed study of the superconducting gap. In tunnel spectroscopy, which measures the one-particle density of states with a high resolution in energy, there is practically no resolution in quasimomentum, i.e., the situation is opposite to that in photoemission spectroscopy [23]. The common limitations of both tunneling and photoemission are the small depth of probing and, as a result, an exceptionally high sensitivity to the properties of the surface and an absence of sensitivity to coherence factors (both methods react to *any* gap in the density of states). The probing depth is much larger in optical experiments, since, due to the low carrier concentration, the light penetrates the HTSC to a depth of about 100 nm. Other decisive advantages of inelastic light scattering are the possibility of probing certain parts of the Fermi surface (by using scattering in different polarizations) and the sensitivity to correlated (coherent) behavior of electrons [24, 25].

The goal of the present review is to analyze the experimental data on Raman scattering of light by electrons, or electronic Raman scattering (ERS), in the superconducting state of HTSC's and to find the relationship between the ERS spectrum characteristics and the symmetry of pairing. For a fuller understanding of the physics of Raman scattering in HTSC, the reader should turn to the reviews in Refs [24–28], which examine the various excitations (phonons, electrons, and spin fluctuations) and present the various theoretical models used in describing the process of inelastic light scattering [29, 30]. The outline is as follows. Section 2 gives a brief history of using ERS in superconductor studies. Section 3 describes the fundamentals of ERS in the normal and superconducting states, while Section 4 provides the relevant information about the experiments. The experimental data on the ERS in different polarizations for crystals with different numbers of cuprate planes and with different levels of doping and disorder are presented in Section 5 which also contains a discussion concerning the data. The section is divided into subsections, each of which systematizes the studies depending on the variable quantity. Section 6 is a discussion of the possible symmetry of the order parameter in HTSC with allowance for the limitations imposed in experiments on the ERS. The last section formulates the main conclusions and problems for the future.

2. Historical survey

The understanding that the Raman scattering spectrum of the superconducting state differs from that of the normal state came fairly early [31]. Nevertheless, the first experimental

attempts to record this difference were unsuccessful [31, 32]. About a decade had to pass before it was understood what superconductivity brings into the spectrum of inelastic light scattering. This was achieved by Abrikosov and Fal'kovskii in their seminal paper [7], where they showed that a new scattering channel related to the breaking of Cooper pairs opens in the superconducting state. As a result of this channel a new peak at the frequency $\Omega = 2\Delta$ emerges in the ERS spectrum, while scattering at frequencies $\Omega < 2\Delta$ is absent for a superconductor with an isotropic gap of the s-type even if such scattering exists in the normal state. The theoretical work that followed took into account the effects of Coulomb interaction and the anisotropy of the Fermi surface [33]. Although the problem had theoretically been solved and the possibility of measuring the superconducting gap with ERS had been proved, the realization of this possibility required additional 20 years, despite the fact that such attempts were made by the leading scientists [34]. The first experiment in which a modification of the ERS spectrum in the superconducting state was observed was carried out with $2H-Nb_2Se$ [35]. This was followed by observations of the superconducting gap in Nb_3Sn and V_3Si [36–38] and by a generalization of the theory to the case of superconductors with a small coherence length [39]. The discovery of high- T_c superconductivity was followed by a report about observing the redistribution of the electron continuum in the superconducting state in the system $Y-Ba-Cu-O$ [40], which was soon corroborated in an independent experiment [41]. The discovery of new superconducting compounds stimulated the development of the theory, and Abrikosov and Fal'kovskii analyzed the scattering for anisotropic superconductors with a small coherence length by studying, in contrast to Klein and Dierker [39], a number of limiting cases [42]. In these experiments new results followed the discovery of new superconductors; the superconducting gap was discovered in the ERS spectra of $Bi_2Sr_2CaCu_2O_{8+x}$ (Bi2212) single crystals with two cuprate planes [43] and of $Tl_mBa_2Ca_{n-1}Cu_nO_{2(n+1)}$ single crystals with one, two, and three CuO_2 planes [44–46], so that by now we have studies of practically all classes of HTSC's.

The polarization features of ERS in the superconducting state, which proved to be extremely informative, had already been studied in the first experiments involving the Y123 and Bi2212 single crystals [47–49]. At the present time we know of detailed polarization investigations of the single crystals $La_{2-x}Sr_xCu_2O_4$ (La214) [50–52], $YBa_2Cu_4O_8$ (Y124) [53, 54], $HgBa_2CaCu_3O_{8+x}$ (Hg1223) [55–57], the electron-type superconductor $Nd_{2-x}Ce_xCu_2O_4$ [58, 59], the fullerene Rb_3C_{60} [60], and the intermetallic compound MgB_2 [61, 62]. The key work in the theoretical understanding of these polarization features is, apparently, that of Devereaux et al. [8], where it was found that the ERS not only makes it possible to measure the superconducting gap magnitude but also provides information about the symmetry of the gap.

3. Theoretical fundamentals of inelastic light scattering in a normal metal and in a superconductor

The Bloch theorem says that each elementary excitation of a medium with translational symmetry can be characterized by a wave vector \mathbf{k} and is represented by a plane wave with the following spatial dependence of the wave function: $\psi_{\mathbf{k}}(\mathbf{r}) = \exp(i\mathbf{k}\mathbf{r})u_{\mathbf{k}}(\mathbf{r})$ [63]. Optical processes in metals and

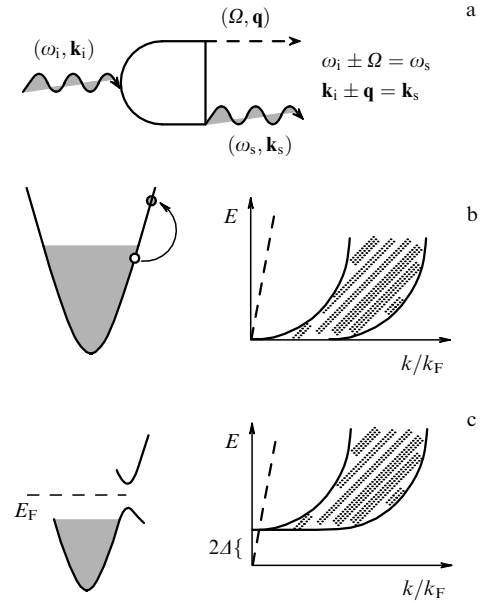


Figure 1. (a) The Feynman diagram of the Raman scattering process. The wave lines represent the photons, while the solid and the dashed lines represent the excitation of the medium. (b) An illustration of the restriction on the phase volume accessible for scattering in a pure metal; (c) the lifting of this restriction for a superconductor.

superconductors are accompanied by creation or annihilation of such excitations, and Raman scattering can generally be defined as the interaction of light with the crystal, in which the radiation of frequency ω_i is transformed into radiation of a new frequency ω_s due to excitation/deexcitation of the medium at a characteristic frequency Ω , which is schematically shown in Fig. 1. The energy and momentum conservation laws determine two scattering channels, the Stokes and the anti-Stokes, which differ in the direction of energy transfer, from the electromagnetic field to the medium and vice versa (usually ERS spectroscopy is limited to Stokes scattering). These kinematic selection rules caused by the homogeneity of the time and the translational invariance of the medium must be supplemented, for a complete description of the process, with symmetry restrictions. In view of the fact that a photon is an odd-parity excitation of the electromagnetic field and that two photons participate in each elementary act, only even-parity excitations of the medium are studied in the Raman scattering. The fact that a relationship between ω_i and ω_s emerges can easily be explained by the theory on the assumption that the optical polarizability α is a function of the generalized coordinate of the excitation, Q , in which the linear relationship between the light field and the medium changes the frequency of the optical field [64].

In the experiment the crystal is irradiated by light from a laser, and the scattered light filtered by a spectrometer is recorded by an optical detector. The detector registers the photons, and the dependence of the number of photons on their frequency $I(\Omega = \omega_i - \omega_s)$ is the Raman scattering spectrum. This spectrum is phenomenologically related to the polarizability α of the crystal and, quantum-mechanically, to the matrix element of the transition responsible for the creation (annihilation) of the excitation. For a metal, the differential scattering cross-section which makes it possible to describe the process without knowing the detailed properties

of the intermediate states, has the form

$$\frac{d^2\sigma}{d\Theta d\Omega} = \frac{r_0^2}{\pi[1 - \exp(-\Omega/T)]} \frac{\omega_c}{\omega_s} \chi''(\Omega, q), \quad (3.1)$$

where $r_0 = e^2/4\pi\epsilon_0 mc^2$ is the Thomson radius of the electron, Θ is the solid angle, and $\Omega = \omega_i - \omega_s$ is the Raman scattering frequency.

In a normal metal, the light scattering is possible on intraband and interband electron excitations, i.e., light scatters on fluctuations of the effective density [33, 65]. The interband contribution is resonant, and allowing for it requires the use of second-order perturbation theory. The intraband contribution is not resonant, and so the use of first-order perturbation theory is sufficient [64]. However, in a pure metal these low-energy excitations are inaccessible for ERS, since for any initial state there is no final state for which the energy and quasimomentum conservation laws hold simultaneously in an elementary scattering act, as illustrated by Fig. 1b. Indeed, for a Fermi liquid with an excitation spectrum of the $E = \mathbf{v}_F \cdot \mathbf{q}$ type, there can be no energy transfer in the limit of vanishing wave vectors, $\mathbf{q} \rightarrow 0$. The reason is the restriction on the phase volume accessible for scattering, with the restriction lifted in the ‘dirty’ limit. Moreover, the finite thickness of the skin layer and the nonparabolic nature of the electron bands also lead to scattering in the normal metallic state [7, 66]; these mechanisms, however, do not explain the scattering in the broad energy range typical of HTSC’s. Note that the change in the kinematic selection rules for a metal is caused by the fact that these rules hold only for transparent media with ideal translation symmetry and with elementary excitations that have an infinite lifetime. In HTSC’s, phonons and impurities caused by the nonstoichiometry and other factors that break the translational symmetry of the crystal lead to a smearing of the wave vector \mathbf{k} for which scattering is allowed [25]. A decrease in the lifetime of quasiparticles in HTSC’s [67] can also lead to a broad electron continuum with a high intensity in ERS spectra, which may be due to spin and charge correlations [68, 69] and/or a large value of the electron–phonon interaction [70, 71]. In addition, electron scattering in the metallic state of HTSC’s can be explained by impurity scattering [72] and the scattering of quasiparticles of a marginal Fermi liquid [73].

The ERS intensity I is proportional to the square of the transition matrix element γ which under certain simplifying assumptions can be reduced to the convolution of the curvature of the conduction band and the unit polarization vectors of the exciting and scattered light:

$$\gamma_{\mathbf{k}} = \frac{m}{\hbar^2} \sum_{\alpha, \beta} e_{\alpha}^s \frac{\partial^2 \epsilon_n(\mathbf{k})}{\partial k_{\alpha} \partial k_{\beta}} e_{\beta}^i. \quad (3.2)$$

This formula is derived in the $\mathbf{k} \cdot \mathbf{p}$ approximation of perturbation theory, which is also known as the effective mass approximation, since the second derivative of the electron excitation energy with respect to the wave vector is the inverse mass of the electron in the crystal. With respect to ERS, the effective mass approximation which can be used only for the nonresonant case and for electrons near the energy extremum in the band, has a transparent physical meaning: the heavy charge carriers have weaker fluctuations and contribute less, since the modulations of the dielectric function are insignificant. Although the applicability of this

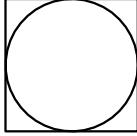
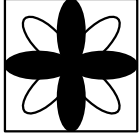

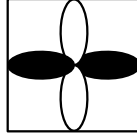
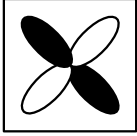
approximation is dubious [25, 68, 72], it is widely used in the description of ERS both in calculations that use the diagrammatic technique [7, 38] and in solving kinetic equations [30].

By examining the symmetry properties of the ERS matrix element it is possible to connect the scattering polarizations under investigation with the various projections of the effective mass tensor on the Fermi surface. Expanding the matrix element in a set of orthonormal functions (usually the harmonics of the Fermi surface are chosen as such a set), we can determine what components of the effective mass tensor contribute to a specific polarization. In most theoretical models used to describe ERS, tetragonal symmetry is predominant. This simplification is justified by the fact that superconductivity is realized in CuO_2 layers with an almost perfectly square lattice for which the crystallographic orthorhombic distortions are small, although the real symmetry of HTSC is usually lower than tetragonal [17]. In this case, for a cylindrical Fermi surface parallel to the c axis with an azimuthal angle φ , the expansion of the ERS matrix element in the Fermi-surface harmonics leads to irreducible representations of A_{1g} , A_{2g} , B_{1g} , and B_{2g} symmetries, which transform as $\cos 4\varphi$, $\cos 2\varphi$, $\sin 2\varphi$, and $\sin 4\varphi$. Table 2 reflects the relationship between the main polarizations used in the experiments and the components of the inverse mass tensor. This table suggests that in the event of crossed polarizations $\mathbf{e}_i \perp \mathbf{e}_s$, the not fully symmetrical components of the inverse mass tensor are measured. Here the B_{1g} -symmetry excitations are measured in the $x'y'$ -polarization in which the parts of the Fermi surface that are probed are those that are close to the principal axes of the Brillouin zone, while for the B_{2g} -symmetry excitations measured in the xy -polarization, the regions of the Fermi surface along the diagonals contribute the most. What is measured in the in-plane polarized spectra ($\mathbf{e}_i \parallel \mathbf{e}_s$) is the fully symmetrical A_{1g} -component of the inverse mass tensor with a mandatory admixture of the not fully symmetrical B -representations, which is determined by the orientation of the electric field. Antisymmetric excitations of the A_{2g} -symmetry are not, in principle, Raman-active, but they may contribute in the case of resonance scattering, which contribution can be isolated by using circularly polarized light [68]. For the three-dimensional case we must add the irreducible representations of the E_g -symmetry, which are measured in the xz - and yz -polarizations. In addition, the increase in the number of dimensions leads to the emergence of an

Table 2. Relationship between the basic polarizations and the components of the inverse mass tensor.

Irreducible representation of group D_{4h}	B_{1g}	B_{2g}	A_{1g}
Schematic representation of polarization			
Harmonics of the Fermi surface			

Table 3. Pairing symmetries and the shape of the gap function in the reciprocal space for states that are candidates for the dominant contribution to pairing.

Irreducible representation	A_{1g}	A_{1g}	A_{2g}	B_{1g}	B_{2g}
Basis function	Constant	$x^2 + y^2$	$xy(x^2 - y^2)$	$x^2 - y^2$	xy
Designation	s	s^*	g	$d_{x^2-y^2}$	d_{xy}
Schematic representation of $\Delta(\mathbf{k})$ in the Brillouin zone					

additional A_{1g} -component in the tensor, which is measured in the zz -polarization.

In the superconducting state, the description of ERS is much simpler, since superconductivity allows for energy transfer without momentum transfer. The reason is that the ground state of a superconductor consists of Cooper pairs [7], and a photon can destroy a pair whose total quasimomentum is zero. The energy $E_{\mathbf{k}}$ needed to destroy the pair may be written, according to the BCS theory, as $E_{\mathbf{k}} = 2(\Delta_{\mathbf{k}}^2 + \epsilon_{\mathbf{k}}^2)^{1/2}$, where $\epsilon_{\mathbf{k}}$ is the quasiparticle energy measured from the Fermi level [5]. Hence, even if the momentum transfer is zero, there can be finite-energy excitations in the superconductor (see Fig. 1c). In the case of an isotropic (s) gap, the transition to the superconducting state manifests itself as complete suppression of scattering in the low-energy part of the ERS spectrum, in which event there is no signal at frequencies $\Omega \leq 2\Delta$ and the signal is singular at a frequency equal to twice the superconducting gap [7]. Thus, in a certain sense the ERS spectrum reflects the density of states of the superconductor with the doubled frequency scale.

ERS for a superconductor with a small coherence length (the typical case for HTSC's) was calculated by Klein and Dierker [39] who found that

$$I = \frac{2\pi N_F}{\Omega} \text{Re} \left\langle \frac{|\gamma_{\mathbf{k}}|^2 |\Delta_{\mathbf{k}}|^2}{\sqrt{\Omega^2 - 4|\Delta_{\mathbf{k}}|^2}} \right\rangle. \quad (3.3)$$

Here N_F is the density of states at the Fermi level, γ is the scattering matrix element, Δ is the superconducting gap, and the angular brackets stand for averages over the Fermi surface. To allow for screening, we write the ERS intensity as a sum of two contributions:

$$I = \left(\langle \gamma^2 \Theta \rangle - \frac{\langle \gamma \Theta \rangle^2}{\langle \Theta \rangle} \right), \quad (3.4)$$

where Θ is Tsuneto's complex-valued function [74] responsible for the singularity in ERS at the frequency equal to 2Δ , with

$$\Theta(\Omega, \mathbf{k}) \propto N_F \frac{4|\Delta_{\mathbf{k}}|^2}{\Omega \sqrt{\Omega^2 - 4|\Delta_{\mathbf{k}}|^2}}. \quad (3.5)$$

Note that because of the full symmetry of Tsuneto's function, the second term on the right-hand side of equation (3.4), which is responsible for screening, leads to the disappearance of superconducting response for fully symmetrical scattering.

Selecting certain polarizations of the exciting and scattered photons \mathbf{e}_i and \mathbf{e}_s , one can, as in the normal state, probe

separate parts of the Fermi surface and determine the superconducting gap on these parts. Obviously, the ERS spectrum will be different for pairing of different symmetry, since the density of the electronic states of a superconductor depends on the symmetry of the superconducting gap. Furthermore, depending on the pairing symmetry, the superconducting gap varies differently over the Fermi surface, which can be explained by the difference in phase factors (Table 3). For instance, in the case of d-pairing the gap depends on the wave vector according to the law $\Delta_d(\mathbf{k}) = \Delta_0(\cos k_x - \cos k_y)$ and is an alternating function of the wave vector, with zeros on the diagonals of the tetragonal Brillouin zone. For s-pairing, which may be isotropic, $\Delta_s(\mathbf{k}) = \Delta_0$, or anisotropic, $\Delta_s(\mathbf{k}) = \Delta_0(\cos k_x + \cos k_y)$, the zeros of the superconducting gap manifest themselves only in the latter case. However, for anisotropic s^* -pairing, the gap vanishes not on the diagonals of the square, $k_x = \pm k_y$, but on the lines $k_x = \pi/8 \pm k_y$, which is necessary for conservation of the rotational symmetry C_4 . Obviously, the largest optical response is observed when the symmetry of the gap and the symmetry of the ERS matrix element coincide. Note that the above formulas suggest that the ERS method is not phase-sensitive. In view of the fact that the formulas for the intensity contain the matrix element squared, inelastic scattering provides information only about the absolute value of the superconducting gap and not about the phase [75]. Nevertheless, since different polarizations of ERS probe different parts of the Fermi surface, we can partially reconstruct the angular dependence of the order parameter by comparing the spectra of different polarizations [8].

4. Experimental details

All the measurements described in the present review were done using single crystals. A detailed description of the experimental setup and the conditions under which the measurements were made can be found in Ref. [76]. The scattering configuration which from now on will be called the scattering polarization, will be presented in Porto's notation: $\mathbf{k}_i(\mathbf{e}_i\mathbf{e}_s)\mathbf{k}_s$. Since the main geometry used to study ERS in HTSC's is that of quasibackscattering, the unit wave vectors of the exciting (\mathbf{k}_i) and scattered (\mathbf{k}_s) light are always antiparallel and point in the directions perpendicular to the plane that contains the polarization vectors. This makes it possible to use the abbreviated notation in which only the polarization vectors \mathbf{e}_i and \mathbf{e}_s are specified. Actually, the angles of incidence (with respect to the normal to the sample's surface) of exciting light used in the experiments are fairly large, so as to prevent the mirror-reflected light from penetrating in the spectrometer, but since the dielectric

constant of HTSC is large, the exciting light enters the sample at a small angle.

To compare the ERS in HTSC crystals of different crystal symmetries in a meaningful manner, it is better to obtain and analyze the experimental data in a coordinate system specified by the orientation of the Cu–O bonds of the cuprate plane [24]. In such a coordinate system (and using the irreducible representations of the tetragonal symmetry group D_{4h}), the B_{1g} -spectra yield information about the superconducting gap along the principal axes of the Brillouin zone, while the spectra of B_{2g} -symmetry, along the diagonals of the zone. The spectra acquired with parallel in-plane polarizations always contain, in addition to the fully symmetrical component, an admixture of the B-components depending on how the electric vector of the photon is directed with respect to the crystallographic directions (B_{1g} for the principal directions and B_{2g} for the directions that form an angle of 45° with the Cu–O bonds). Hence, isolating the in-plane A_{1g} -component of scattering requires carrying out measurements in two polarizations. For out-of-plane spectra in which one of the polarization vectors is perpendicular to the basal plane, each spectrum contains scattering of only one symmetry. Thus, the zz -spectra contain only the A_{1g} -component, while the zx - (zy)-spectra represent the E_g -symmetry excitation.

Even light from a laser of moderate power may significantly change the temperature of the sample, especially in the superconducting state [44, 77, 78]. Hence overheating must be minimized by measuring the actual temperature from the ratio of the Stokes and anti-Stokes scattering components. The spectra measured at a temperature T are given either in the form $I(\Omega, T)$, where the intensity I is the number of detected photons at the frequency $\omega_s = \omega_i - \Omega$, or in the form of ERS susceptibility:

$$\chi''(\Omega, T) \propto \frac{I(\Omega, T)}{1 - \exp(-\hbar\Omega/k_B T)}. \quad (4.1)$$

Obviously, for low-temperature spectra $I(\Omega, T \rightarrow 0)$ and $\chi''(\Omega, T \rightarrow 0)$ are practically indistinguishable.

Since the scattering cross-section for HTSC's is much smaller than the scattering cross-section for dielectric oxide phases, even a small number of such phases may considerably distort the ERS spectrum. Hence special attention should be paid to the quality of the samples and the absence of a layer of adsorbate on the sample surface at low temperatures.

5. Experimental results and discussion

The Raman scattering spectrum of any HTSC consists of an intense electron continuum on which there are narrow phonon lines. The main contribution to the scattering is provided by the electron component which dominates in the spectrum up to energies higher than 1 eV [79–81], while the phonon component contains a sizable part of the spectral weight only at low frequencies. Superconductivity considerably modifies the ERS spectrum at frequencies not exceeding 800 cm^{-1} , a fact illustrated by Fig. 2 which shows the spectra of three different symmetries for the Bi2212 single crystal in the normal and superconducting states. Comparison of these two states shows that superconductivity leads to suppression of scattering (in fact, incomplete suppression) at low frequencies and a peak Ω_{\max} at high frequencies. The other characteristic energies in the spectrum are the points where

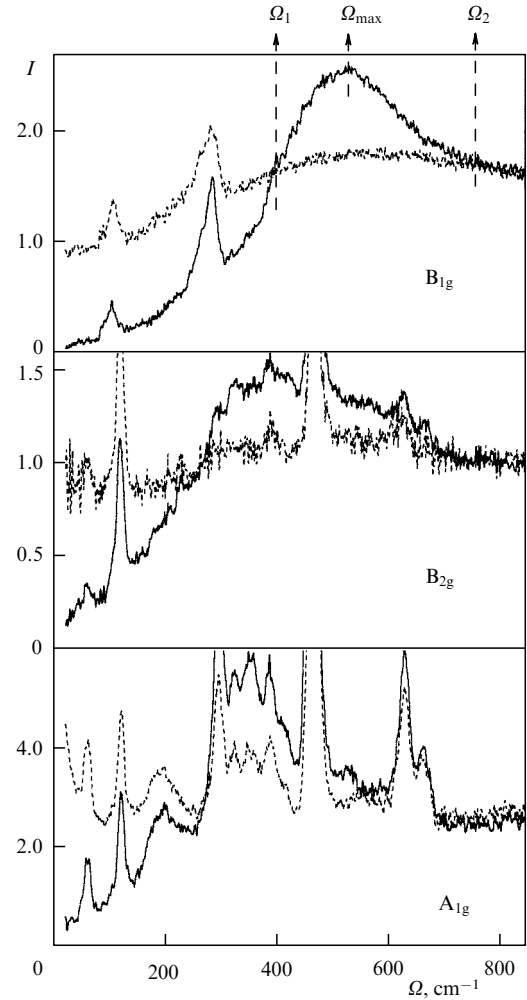


Figure 2. ERS spectra of different symmetries for the normal ($T = 100 \text{ K}$, dashed curves) and superconducting ($T = 10 \text{ K}$, solid curves) states produced in excitation with $\lambda = 488 \text{ nm}$ in an optimally doped ($T_c = 91 \text{ K}$) single crystal Bi2212. The arrows in the B_{1g} -symmetry spectrum mark the characteristic frequencies Ω_1 , Ω_2 , and Ω_{\max} (see explanation in the main text).

the normal and superconducting spectra intersect, Ω_1 and Ω_2 . The first point, Ω_1 , determines the region $\Omega < \Omega_1$, where the scattering in the superconducting state decreases. The second point determines the region where the scattering increases, $\Omega_1 < \Omega < \Omega_2$, and divides the region that is not modified by superconductivity, $\Omega > \Omega_2$. Since most theoretical models do not account for scattering in the normal state and since the superconductivity-induced changes in the electron continuum are moderate, often the analysis of the ratio of the ERS susceptibilities in the superconducting and normal states, χ''_s/χ''_n , proves to be informative. (Figure 3 shows the behavior of the ratio for three different symmetries.) The general interpretation of the ratio χ''_s/χ''_n is not really very complicated. At high frequencies $\Omega > \Omega_2$ the scattering spectra in the normal and superconducting states coincide and the susceptibility ratio is equal to unity. As the frequency decreases, we land in the range of energies close to 2Δ , in which the scattering in the superconducting state considerably exceeds the scattering in the normal state. Accordingly, the susceptibility ratio χ''_s/χ''_n exceeds unity for frequencies $\Omega_1 < \Omega < \Omega_2$. At lower frequencies, $\Omega < \Omega_1$, the spectra of the superconductor become less intense than the spectra in the

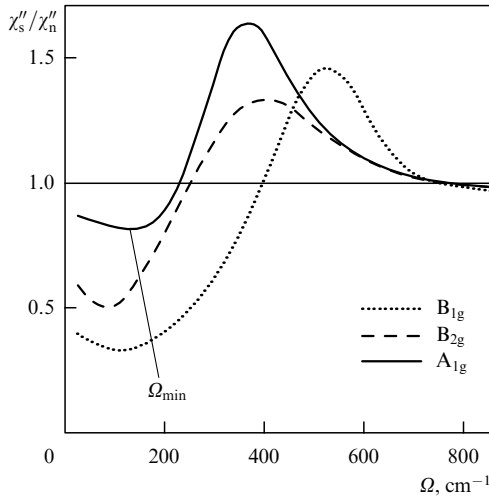


Figure 3. Ratio of ERS susceptibilities, χ''_s/χ''_n , in the normal and superconducting states for different scattering symmetries (indicated in the figure) in Bi2212.

absence of superconductivity, since the states with such energies are pushed out into the region of higher energies when the superconducting gap opens. Here $d\chi''_s/d\Omega > d\chi''_n/d\Omega$, and χ''_s/χ''_n decreases at lower frequencies. However, starting at a certain frequency Ω_{min} , the susceptibility ratio again begins to increase, which is an indication that the slope of the superconducting spectrum has become smaller than that of the normal spectrum, $d\chi''_s/d\Omega < d\chi''_n/d\Omega$. As we will see shortly, in some cases the analysis of χ''_s/χ''_n provides additional information about the features of ERS in HTSC's [76].

Since the phase diagram of HTSC's is fairly complicated, we will examine the experimental results for each region of this diagram separately. Moreover, since crystal anisotropy is the cause of the strong anisotropy of the normal and superconducting dynamics of the carriers in the basal plane and perpendicular to that plane, the spectra of the in-plane and out-of-plane configurations of scattering will also be examined separately. We will also separate the effect of the resonant and temperature conditions and the effects caused by impurities.

5.1 Electronic Raman spectra at optimal doping

Analysis of the data in Fig. 2 shows that ERS in HTSC's has features that set it apart from ERS in the classic superconductors studied earlier [35–38]. First, complete suppression of scattering at low frequencies has never been observed for studied polarizations. Second, for spectra of different symmetries the peaks in ERS in the superconducting state are at different frequencies. Third, the low-frequency parts of the spectrum and the static limits of the ERS susceptibility are also polarization-dependent. All these differences are manifestations of the modified pairing mechanism and a more complicated structure of the order parameter, compared to classic superconductors. The first difference suggests the presence of zeros (nodal structure), and the second and third suggest that the order parameter is highly anisotropic. Although there is still no agreement as to what peak is related to the superconducting gap (some researchers prefer the B_{1g} -symmetry peak [8], others the A_{1g} peak [75]), it must be noted that the superconducting gap determined from the

arrangement of the ERS peaks is usually much larger than the BCS gap of the weak-coupling model. Indeed, if we associate the superconducting gap with the position of the peak in the low-temperature ERS spectrum, then in Bi2212 at optimal doping we have $2\Delta/T_c \approx 8.0$ for the B_{1g} channel of scattering, approximately 5.5 for the A_{1g} channel, and about 6 for the B_{2g} channel, while the gap's anisotropy is determined from the ratios $B_{1g}/B_{2g} \approx 1.2$ and $B_{1g}/A_{1g} \approx 1.35$. Such degrees of anisotropy are observed for doping levels that do not deviate significantly from those for optimal doping for Y123, La124, Tl2201, and Hg1223 [44, 47, 50, 55].

Figure 2 shows that the superconductivity-induced changes for the A_{1g} -symmetry spectrum are, at least, no smaller than those for B_{1g} , while the theory [see equations (3.3) and (3.5)] predicts total screening for the fully symmetrical response [33, 39]. Despite the numerous attempts [82–84] to explain the existence of strong scattering for fully symmetrical superconducting spectra, not a single one of such explanations can be called generally accepted [85], and this feature of the polarization dependence has yet to be clarified. Nevertheless, it must be noted that the intensity of the superconducting peak usually correlates with the intensity of the normal continuum: the stronger the normal scattering, the higher the superconducting peaks. This is clearly seen in the behavior of the susceptibility ratio χ''_s/χ''_n depicted in Fig. 3, where the relative intensity of the peaks varies under symmetry variations much weaker than the variations of the susceptibilities themselves.

Such HTSC's as Bi2212 and R123 (*R* stands for a rare-earth element) have an orthorhombic structure which is described by the point group D_{2h} . For Bi2212, an incommensurate modulation along the direction *b* in BiO layers leads to a difference in the lattice constants *a* and *b*. For R123, a lattice distortion is caused by one-dimensional CuO chains which contribute substantially to ERS, so that the *yy*-polarization spectrum is much stronger than that of the *xx*-polarization [87–91]. An important difference between these two orthorhombic structures is that the direction of the nonequivalent *a* and *b* axes coincides with the direction of the Cu–O bonds in R123 but not in Bi2212. This has serious consequences for the symmetry of the order parameter in both HTSC's and can be the reason for the difference in the low-frequency parts of the spectrum [72, 90]. Studies of nontwinned single crystals Y123 [91] and Bi2212 [92] have shown that there is no *x*–*y* anisotropy of the gap for the real part of the gap but that there could be such an anisotropy for the imaginary part. Indeed, comparison of the $A_{1g}(xx)$ - and $A_{1g}(yy)$ -spectra shows that the low-temperature fully symmetrical ERS peaks are located at the same frequency in both polarizations, although their intensities are different.

Note that the ERS polarization dependences differ significantly for the electron-type superconductor $\text{Nd}_{2-x}\text{Ce}_x\text{Cu}_2\text{O}_4$ [58, 59] and for the recently discovered intermetallic superconductor MgB_2 [61, 62] with a critical temperature of 39 K. For $\text{Nd}_{2-x}\text{Ce}_x\text{Cu}_2\text{O}_4$, in the first studies the gap's anisotropy determined from the ratio $B_{1g}/B_{2g} \approx 1.0$ proved to be within $4.1 < 2\Delta/T_c < 4.9$, which suggested that the pairing symmetry in the given compound belonged to the *s*-type. However, one of the main features that distinguishes electron-type HTSC's from hole-type HTSC's is the exceptionally narrow interval of allowed doping levels within which superconductivity is possible (e.g., for the material in question this interval is $0.10 < x < 0.14$ [86], while for the hole-type La214 it is

$0.05 < x < 0.3$ [51, 52]). Later we will see that for doping levels far from the value that ensures maximum transition temperatures, the ERS anisotropy may become much smaller. Indeed, recent studies conducted by Blumberg et al. [59] support the idea that there is polarization anisotropy of scattering in $\text{Nd}_{2-x}\text{Ce}_x\text{Cu}_2\text{O}_4$. What is interesting is that the ratio B_{1g}/B_{2g} obtained in this study is smaller than unity: $B_{1g}/B_{2g} \approx 0.75$ and $3.3 < 2\Delta/T_c < 4.4$. To make these results agree with the data on hole-type superconductors, in which $B_{1g}/B_{2g} \geq 1$, Blumberg et al. [59] proposed a hypothesis about a nonmonotonic superconducting gap of the d-type. Note that such a superconducting gap was proposed earlier in Refs [93, 94] to explain the resonance dependence of ERS. As for MgB_2 , the ERS superconducting spectra recorded for polycrystals in crossed and parallel polarizations suggest that the superconducting gap has two components, $\Delta_{\min} \approx 22 \text{ cm}^{-1}$ and $\Delta_{\max} \approx 50 \text{ cm}^{-1}$, but the two peaks are observed in both crossed and parallel polarizations [61]. Studies conducted with single crystals revealed a small polarization anisotropy for the high-energy peak, while no low-energy peak was recorded [62].

Low-temperature ERS spectra with doping close to the value that ensures a maximum transition temperature T_c are now the most thoroughly studied spectra. They are rather similar in the polarization anisotropy of the peaks, irrespective of the type of compound and the number of cuprate planes [24, 95]. Indeed, for La214 with a single cuprate plane and $T_c = 37 \text{ K}$, the gap anisotropy $B_{1g}/A_{1g} \approx 1.6$ and the ratio $2\Delta/T_c$ is equal to 8.1 and 5.1 for the B_{1g} and A_{1g} channels of scattering [50, 52], while for Hg1223 with three CuO_2 planes and $T_c = 134 \text{ K}$, the gap anisotropy $B_{1g}/A_{1g} \approx 1.5$ and the ratio $2\Delta/T_c$ is equal to 9.3 and 6.4 for the same symmetries [55]. The discrepancy in polarization anisotropy for different HTSC's with roughly the same doping levels does not exceed the variance of the results obtained by different groups of researchers studying the same compound. On the basis of this similarity of spectra it is only natural to assume that the cuprate planes, common for all HTSC's, provide the main contribution to low-temperature scattering. And although the question of the origin of the strong, nearly frequency-independent scattering in the normal metallic state remains unresolved, notwithstanding the multitude of hypotheses concerning the origin, the very fact that the intensities of the superconductivity-induced peaks are proportional to the intensities of the normal continuum suggests that the latter are generated by the same states that participate in superconductivity and belong to the CuO_2 planes.

Analysis of low-temperature ERS spectra suggests that the superconducting gap of the CuO_2 plane is anisotropic at optimal doping and has zeros on the Fermi surface. Here the superconducting gap is largest along the directions of the $\text{Cu}-\text{O}$ bonds and smallest along the $\text{Cu}-\text{Cu}$ directions. The polarization dependence and the cubic increase of intensity at frequencies lower than Ω_{\max} were explained for Bi2212 on the assumption that the gap has $d_{x^2-y^2}$ -symmetry [8]. However, such symmetry was questioned in research containing indications that ERS does not 'detect' the phase of the order parameter and, as a result, cannot distinguish between a d-gap and an anisotropic s^+ -gap [75, 90, 96]. Nevertheless, today most of the researchers agree that at optimal doping the main contribution to pairing occurs in the d channel [24].

5.1.1 B_{1g} -symmetry scattering. An interesting feature of low-temperature ERS spectra is the dependence of the scattering

intensity at frequencies lower than the maximum of the electron peak, Ω_{\max} [8]. Figure 2 shows that for Bi2212 the intensity increases with frequency according to the cubic law $I \propto \Omega^3$ for the B_{1g} -symmetry spectra, while for the spectra of other symmetries intensity increases linearly with frequency, $I \propto \Omega$. It was the cubic dependence that suggested that the d-symmetry channel is the dominating component of pairing in HTSC's. The origin of the cubic dependence can easily be understood by examining equation (3.4) for $d_{x^2-y^2}$ -symmetry pairing. Indeed, since the matrix elements of the A_{1g} - and B_{2g} -symmetries are finite near the zeros of the $d_{x^2-y^2}$ -gap, the density of states, which is proportional to the energy, determines the low-frequency response of the given scattering channels. However, both $\Delta(\mathbf{k})$ and $\gamma_{B_{1g}}(\mathbf{k})$ vanish at the same point of the Fermi surface, which leads to a cubic dependence in which the matrix elements contribute Ω^2 and the density of states Ω . Thus, the \mathbf{k} -dependence of the gap and the ERS matrix element may help in determining the positions of the zeros of the order parameter.

Note, however, that not all HTSC's exhibit such a cubic dependence for the low-frequency part of the B_{1g} -spectrum. The absence of such a dependence has been reliably established for the system Y123 [72, 75] in which, in addition to conducting CuO_2 planes, there are conducting CuO chains. Figure 4 shows the B_{1g} -spectra of optimally doped single crystals Nd123 and Bi2212 , which demonstrate a remarkable difference in the low-frequency responses. While for Bi2212 the characteristic feature of its spectrum is its convexity at low frequencies, which is indicative of a nonlinear dependence, for Nd123 the low-frequency part of the spectrum is linear in frequency [75, 90, 97, 98]. This difference becomes even more evident when the spectra are represented on the log-log scale (Fig. 4b). Comparison of the slopes of the low-frequency parts suggests that the exponent for Bi2212 is approximately three times larger than that for Nd123 . The spectral region in which a deviation from the cubic dependence is observed yields another characteristic frequency Ω^* which for Bi2212 does not exceed 0.2Δ at a given excitation energy.

The difference in the low-frequency regions of the B_{1g} -spectra for Bi2212 and R123 is probably caused by the difference in the nature of the orthorhombic distortions. As noted earlier, in Bi2212 these distortions do not lead to a loss of the symmetry plane σ_v and, as a result, the $d_{x^2-y^2}$ - and s-components of the order parameter belonging to different irreducible representations (B_{1g} and A_g) of the orthorhombic group cannot mix and the zeros of the ERS matrix element remain on the diagonals of the Brillouin zone. In R123 crystals, the orthorhombic distortions introduced by the CuO chain lead to a loss of the above-mentioned planes. In this case, the d- and s-components mix, since they belong to the same fully symmetrical representation of the group C_{2v} , and the zeros of the ERS matrix element are displaced from the diagonals of the Brillouin zone. As a result, within the region of the order-parameter zeros, the B_{1g} -symmetry matrix element is nonzero and the intensity of low-energy scattering is determined by the density of states [72].

Much more troubling is the fact that the tetragonal superconductors Ti2201 [44] and Hg1223 [55] exhibit an absence of the cubic component. In the case of Ti2201 this can be explained by the fact that the tetragonality of the given crystals was not specifically checked and weak orthorhombic distortions could have led to a loss of the cubic dependence. For Hg1223 with the doping level close to optimal, the low-frequency B_{1g} -symmetry response was strictly linear in an

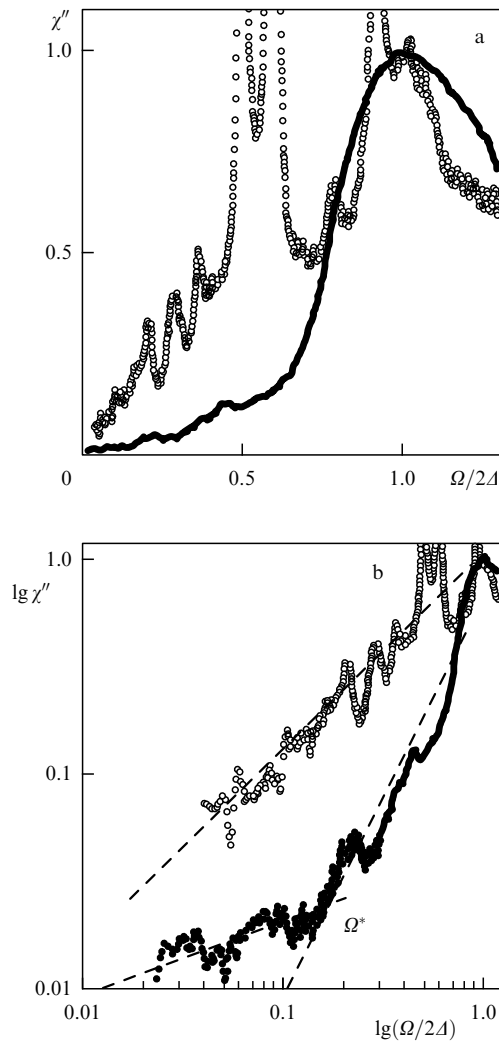


Figure 4. B_{1g} -symmetry ERS spectra at $T = 5$ K for optimally doped Nd123 (open circles) and Bi2212 (full circles) on the ordinary (a) and log-log (b) scales. The results of fitting by a linear function extrapolated to zero frequencies is represented by straight dashed lines, and Ω^* is the crossover frequency (see explanation in the main text).

extremely broad frequency range, but a small cubic component was discovered in underdoped crystals [56].

In any case, only Bi2212 crystals exhibit an almost purely cubic contribution. This may be caused partially by the fact that crystals of the given system easily split in the direction perpendicular to the c axis and that the quality of their surface is practically ideal for optical experiments. Moreover, it must be noted that along with orthorhombic distortions, impurities [76] and temperature [99] may greatly affect the low-energy part of the ERS spectrum.

5.1.2 Effect of impurities on light scattering in the superconducting state. For classic superconductors, the effect of impurities on superconductivity has been established fairly thoroughly. Magnetic impurities lead to depairing and strongly suppress T_c , while nonmagnetic impurities have only a small effect on the critical temperature and lead only to a more isotropic gap. For HTSC's, nonmagnetic impurities suppress T_c no less effectively than magnetic impurities [100], which may serve as an indirect indication of the unconventional symmetry of the order parameter.

Nonmagnetic impurities in d-type superconductors lead to a finite density of states at the Fermi level [101]. This leads to important consequences which make it possible to distinguish between d- and s^* -type pairing. Impurities in the d-superconductor leave the superconducting state gapless, while in the anisotropic s^* -superconductor a gap opens over the entire Fermi surface, with the gap magnitude increasing with impurity concentration [102, 103]. Impurities in d-type superconductors may also lead to localization [104], i.e., quasiparticles with energies below the mobility threshold may be strongly localized. Here the size of the mobility threshold may constitute a considerable fraction of Δ , provided that scattering is in the unitary limit. One of the consequences of localization is the universal saturation of conductivity, in which case conductivity is independent of the impurity concentration. Saturation of this type is observed directly in the IR spectra [105], and the temperature dependence of microwave conductivity and thermal conductivity is an indirect indication of the existence of universal saturation [106]. Universal saturation which is the consequence of the balance between the finite density of states at the Fermi level and the modified quasiparticle lifetime, can occur only if the order parameter has zeros.

As noted earlier, the ERS is not a phase-sensitive method, with the result that in a conventional experiment it cannot unambiguously distinguish between d- and s^* -types of pairing [75]. Nevertheless, the method is sensitive to the presence of zeros of the order parameter and its anisotropy. These characteristics, when combined with the variable impurity concentration, may assist in determining the pairing symmetry in HTSC's [107, 108]. Theoretical studies of superconductors of d-type and anisotropic s^* -type have revealed a difference that should manifest itself in changes that occur in the anisotropy of the ERS peaks and in the low-energy scattering in different polarizations. It was found that impurities in d-type superconductors do not affect the anisotropy of the ERS peaks of different symmetries but that they do modify the low-frequency part of the B_{1g} -spectrum so that the spectral weight is shifted to higher frequencies. Impurities in anisotropic s^* -superconductors decrease the polarization anisotropy of the gap in such a way that the ERS peaks of different symmetries emerge at the same frequency. Here the spectral weight at low frequencies increases and, beginning at a certain impurity concentration, a threshold (the absence of scattering) emerges in the low-frequency part of the spectrum. Furthermore, it was found that, in addition to providing the possibility of distinguishing between d- and s^* -gaps, the effect of impurities on ERS makes it possible to determine the fraction of s-type pairing for a mixed order parameter with preferable d-type pairing [109]. This unique capability of ERS is also caused by the symmetry aspects of the scattering. As noted earlier, B_{1g} -symmetry scattering probes the principal axes of the Brillouin zone, where the d-gap reaches its maximum values, and does not 'see' the diagonals, on which the zeros of the order parameter are located. As a result, for this polarization the slope

$$S = \left. \frac{d\chi''(\Omega)}{d\Omega} \right|_{\Omega \rightarrow 0}$$

of the ERS susceptibility in the superconducting state is proportional to the impurity concentration n_i . The situation is just the opposite for B_{2g} - and A_{1g} -symmetry scattering which probes the region of zeros of the order parameter. In

this case the slope S is independent of the impurity concentration in the superconducting state, i.e., universality is present. In the case of an anisotropic s^* -gap, universality must be observed both for B_{2g} - and A_{1g} -scattering and for B_{1g} -scattering. The reason is that the zeros are in the positions $n\pi/8$ and contribute to the scattering of all symmetries. However, in the case where the zeros are slightly shifted from the diagonals (e.g., due to an admixture of the s -component of pairing), B_{1g} -symmetry scattering begins to ‘see’ the region of zeros, and this ability to ‘see’ depends on how far away from the diagonals the zeros are. Hence for the mixed order parameter $\Delta_{\mathbf{k}} = \Delta_0[\cos(2\varphi) + \alpha]$, the static limit of the ratio of ERS susceptibilities in the superconducting and normal states, χ''_s/χ''_n , for B_{1g} -scattering makes it possible, in principle, to determine α [109].

Experimental verification of the above theories has been conducted for Bi2212, with iron being the impurity, which for the given compound is a substitute for copper in the CuO_2 plane [76, 110, 111]. The behavior of the susceptibility ratio χ''_s/χ''_n for spectra of B_{1g} - and A_{1g} -symmetries in Bi2212 crystals with different iron contents is shown in Fig. 5. If we compare the patterns, we see that the presence of impurities leads to the disappearance of the fully symmetrical 2Δ peak, while the effect of impurities on the superconducting peak of B_{1g} -symmetry is not expressed so vividly. Despite the fact that the increase in impurity concentration changes T_c by 30%, the changes in the positions of the ERS peaks of A_{1g} - and B_{1g} -symmetries occur consistently (Fig. 6). As a result, the polarization anisotropy of the ERS peaks is independent of the impurity concentration, i.e., $\Omega_{B_{1g}}/\Omega_{A_{1g}}$ remains equal to 1.35. Moreover, not a single polarization studied so far has revealed any gap in the low-frequency part of the spectrum. These facts suggest that there is d -symmetry pairing. Deve-

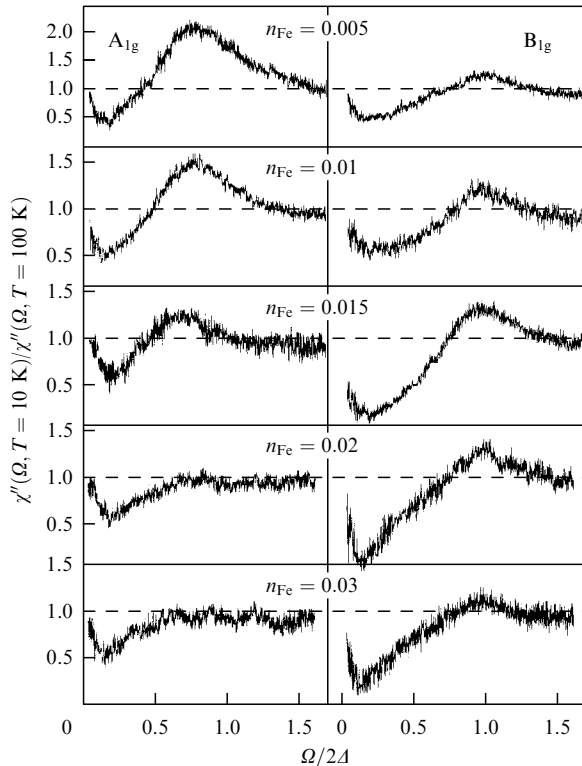


Figure 5. Ratio χ''_s/χ''_n for different iron-impurity concentrations in Bi2212 for two different symmetries.

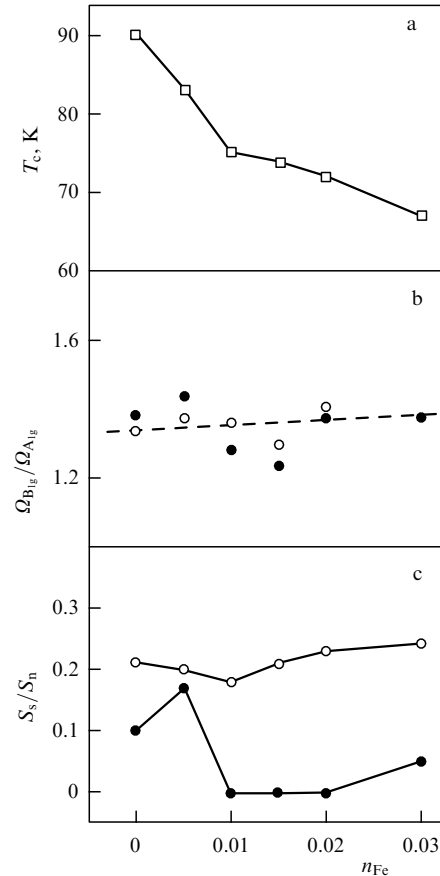


Figure 6. Critical temperature T_c (a), polarization anisotropy ratio $\Omega_{B_{1g}}/\Omega_{A_{1g}}$ (Ω_{\max} is denoted by open circles and Ω_1 by full circles) (b), and the ratio S_s/S_n of the static limits of susceptibility (A_{1g} is denoted by open circles and B_{1g} by full circles) (c), as functions of the impurity concentration in Bi2212.

reaux [112], who assumed that the different oxygen contents in the crystals under investigation can be reduced to different concentrations of impurities (defects), arrived at a similar conclusion while analyzing the B_{1g} -spectra of Bi2212 crystals with three different doping levels. Since a change in the impurity concentration, which violates the charge balance in the system, leads to a change in the doping level, the overall ERS intensity varies depending on the extent of substitution. These changes make comparison of the low-frequency parts of the spectrum more difficult. However, if we normalize the frequency scale and the relative intensities, comparative analysis of B_{1g} -spectra shows that with increasing impurity concentration the spectral weight at low frequencies most likely increases (Fig. 7). It is very difficult to say anything more certain here, since in the given spectral region the phonon scattering provides a contribution that is difficult to account for. Nevertheless, all the data suggest that there is d -symmetry pairing. However, the crossover frequency Ω^* at which the linear dependence is transformed into the cubic dependence, decreases with increasing intensity of impurity scattering, which contradicts the theoretical prediction, namely, an expected increase in the given characteristic frequency for a d -symmetry superconductor [108]. The possible reasons for this discrepancy between theory and experiment are that the impurity has spin and that the doping level changes under substitution (these facts were not taken into account by the theory).

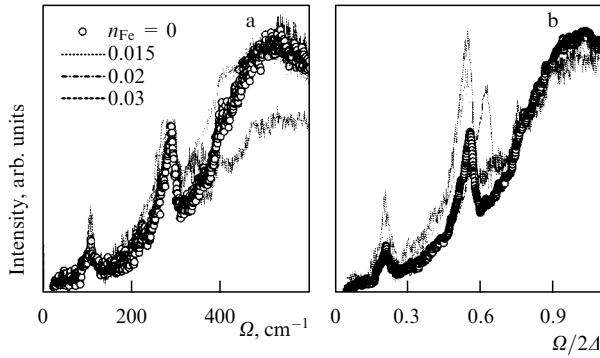


Figure 7. Comparison of the low-frequency part of the B_{1g} spectra of Bi2212 with different impurity concentrations: (a) ordinary case and (b) normalized case.

Studying the ratio χ''_s/χ''_n of susceptibilities in the superconducting and normal states for different doping levels also makes it possible to do a more thorough analysis of the low-frequency part of the spectrum, $0 < \Omega < \Omega_1$. The measurement of static limits shown in Fig. 6c indicates that universality, within experimental error, is observed not only for fully symmetrical scattering, but also for B_{1g} -symmetry scattering. This suggests that the zeros of the superconducting gap either are shifted from their positions on the diagonals of the Brillouin zone or manifest themselves within an extended region near the diagonals. In the first case we can speak of a multicomponent structure of the order parameter ($d+s$) in Bi2212 and of a nonzero integral of the order parameter over the Fermi surface. In the second case, the integral over the Fermi surface is equal to zero, which means there is pure d -pairing [113, 114].

5.1.3 Temperature dependence in the superconducting state.

Since the ERS makes it possible to carry out measurements of the superconducting gap, it would be interesting to study the temperature dependence of this important quantity for HTSC's. For classic superconductors and the intermetallic superconductor MgB_2 , the changes in the positions of the superconductivity-induced peaks agree with the BCS dependence of the superconducting gap [37, 62]. However, the first researchers who investigated Y123 [47] and Bi2212 [49, 115] crystals discovered a sizable departure of the temperature dependence of the ERS peaks from that predicted by the BCS theory, and later detailed studies of La214, Bi2212, and Hg1223 corroborated this anomaly [50, 55, 99].

To demonstrate the anomalous temperature dependence of the ERS peaks, we briefly discuss the result of low-temperature studies of the optimally doped single crystal Bi2212 [94, 99]. Since, for such crystals, the resonance profiles of the B_{1g} -symmetry phonon and electron scattering differ [117–119], the spectrum excited by the light from a He–Ne laser ($\lambda = 633$ nm) contains only the electron component of scattering. Such spectra make it possible to study the temperature dependence of the electron continuum without removing the phonons, i.e., without distorting the electron peaks. Figure 8 which shows several B_{1g} -spectra measured at different temperatures, illustrates the temperature dependence of scattering. The cubic-law increase and the superconductivity-induced peak, both very evident at low temperatures, become less and less pronounced as we approach T_c . A comparison of the spectra shows that the

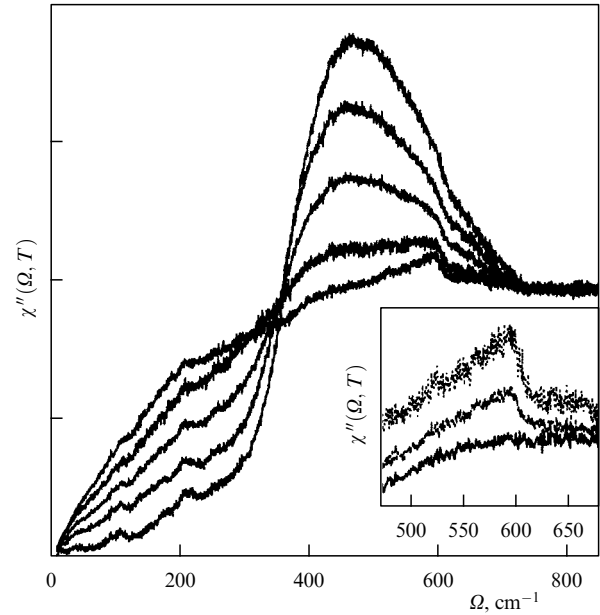


Figure 8. Temperature dependence $\chi''(\Omega, T)$ for B_{1g} -symmetry in optimally doped Bi2212 excited by light with $\lambda = 633$ nm at temperatures below T_c (from top downward: $T = 10, 40, 60, 80$, and 90 K). The inset shows the region of the 2Δ peak at temperatures above T_c (from top downward: $T = 295, 130$, and 100 K).

positions of the 2Δ peaks in the superconducting state are almost independent of temperature. The accuracy in determining the maximum for broad and asymmetric peaks is not very high. However, one more indication of the absence of a strong temperature dependence is that the position of the point Ω_1 , where the normal and superconducting spectra intersect, varies by no more than 10% as the temperature drops from 90 K to 10 K. To illustrate the temperature dependence of the gap, Fig. 9a shows the normalized temperature dependence of the frequencies Ω_1 and Ω_{max} , which suggests that there is a departure from the BCS dependence (the dashed curve) at temperatures close to T_c . The frequencies Ω_1 and Ω_{max} indicate that the peak caused by the breaking of Cooper pairs emerges in a superconducting transition at a nonzero frequency that does not differ too strongly from the frequency realized at the lowest temperature that can be reached in the experiment. At the same time, the intensity of the peak increases significantly as the temperature decreases (Fig. 9b).

Phononless spectra also make it possible to follow the variations of the integrated scattering intensity with temperature. This intensity begins to change when the crystal undergoes a transition to the superconducting state and increases almost linearly in the superconducting state. Such behavior follows from the fact that as the temperature decreases the integrated scattering intensity between Ω_1 and Ω_2 increases more rapidly than the integrated scattering intensity between 0 and Ω_1 decreases (Fig. 9b). Changes in the integrated intensity in the normal state are insignificant, although theoretically for ERS there are no special grounds for introducing a sum rule and postulating the temperature-independent nature of ERS [65, 120]. Nevertheless, the breakdown of the 'sum rule' in the superconducting state attests to the fact that the ERS is sensitive to the coherence factors of the superconducting state and not only to the modification of the electronic states near the Fermi level. In

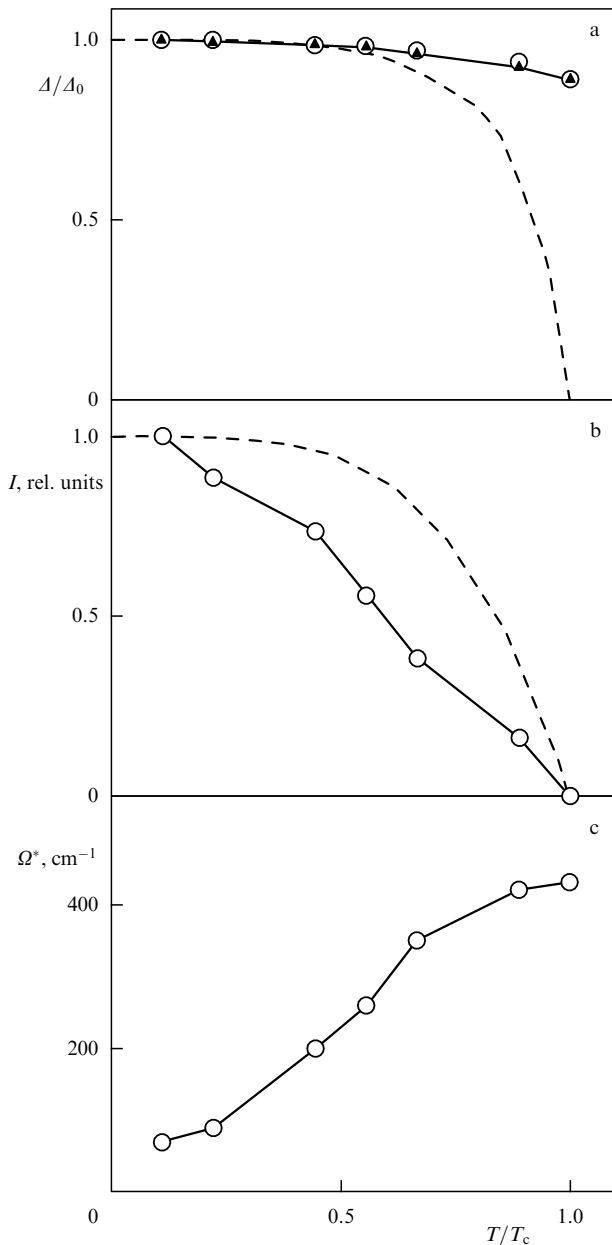


Figure 9. Temperature curves for the parameters of B_{1g} -symmetry spectra. (a) Normalized frequencies Ω_{\max} (open circles) and Ω_1 (full triangles) and the BCS dependence of the superconducting gap (dashed curve). (b) Normalized integrated intensity (open circles) and the dependence of the order parameter of the two-fluid model (dashed curve). (c) The crossover frequency Ω^* .

a superconductor, the electron continuum existing in the normal state not only is redistributed from low frequencies to higher frequencies but also gets stronger, with the greatest perceptible change occurring in the frequency range corresponding to the response of the superconducting condensate. This last factor stems from the phase coherence of the condensate and differs substantially from the behavior of the response to the emergence of a pseudogap which is also recorded in ERS mainly for lightly doped HTSC's. When the pseudogap emerges, at a temperature $T^* > T_c$, there occurs a loss in spectral weight at some frequencies caused by the disappearance of a fraction of the Fermi surface. Since the pseudogap state is not coherent, one observes only a decrease in the scattering intensity without any compensation at other

frequencies. Comparing the ERS for the superconducting and pseudogap states shows that the method is sensitive to the coherence of the investigated state. This dependence on the coherence factors sets ERS spectroscopy apart from angle-resolved photoemission and tunnel and infrared spectroscopies which measure any gap in the excitation spectrum. In the photoemission and tunnel spectroscopies, this is because the one-particle density of states is measured, while in the infrared spectroscopy this is due to symmetry limitations, since this method involves measuring correlation functions of the current–current type, which are odd functions.

An interesting aspect concerning the studies of the temperature dependence of ERS is the possibility of following the temperature evolution of the crossover frequency Ω^* at which the linear dependence transforms into the cubic dependence in the low-frequency part ($\Omega < \Omega_{\max}$) of the B_{1g} -spectrum. Figure 9c shows the dependence of Ω^* on the reduced temperature. We see that near T_c in the low-frequency part of the spectrum the linear dependence is predominant. This could imply that the zeros of the order parameter on the Fermi surface are of an extended nature, at least at temperatures close to T_c . Thus, the superconducting gap in HTSC's demonstrates a temperature behavior that differs from that of the BCS gap. In view of the fact that in the self-consistent equation for the energy gap the temperature and wave-vector dependences factorize, the anisotropy of the BCS gap does not depend on temperature and the BCS gap evolves with temperature without changing its shape in \mathbf{k} -space. Interestingly, the anisotropy of the gap in the intermetallic compound MgB_2 is also temperature-dependent [62].

Summarizing Section 5.1.3, we can say that the temperature dependence of ERS in the superconducting state suggests that (1) the gap determined from the position of the 2Δ peak and/or points where the normal and superconducting spectra intersect differs substantially from the BCS temperature dependence in the weak-coupling limit, (2) superconductivity leads to violation of the optical 'sum rule', and (3) the cubic component of the B_{1g} -spectrum begins to dominate at temperatures much lower than the superconducting transition temperature.

5.1.4 Resonance properties. Despite the importance of establishing the resonance properties of ERS, there are very few works describing investigations in which the frequency of the exciting light is varied [94, 115–119, 121]. Researchers have established without a doubt that ERS in the normal state of HTSC's is of a resonant nature, since for all polarization the scattering intensity depends on the wavelength of the exciting light and usually increases with the light's frequency. The importance of the resonance stems from the fact that the scattering proceeds through real electronic states, with the result that the band structure must be taken into account [120, 122]. The intensity of the ERS peaks in the superconducting state also demonstrates its resonant nature which in many respects is similar to the resonance in the normal state. An interesting feature of the resonant behavior of superconducting peaks is the change in the spectral shape of the superconductivity-induced peaks, which manifests itself most vividly at frequencies $\Omega < \Omega_{\max}$, and in the very position of the peak at Ω_{\max} [55, 94, 121]. At high excitation energies the low-frequency part of the scattering is characterized by large values of $d\chi''_s/d\Omega$, and the peaks are shifted into the high-

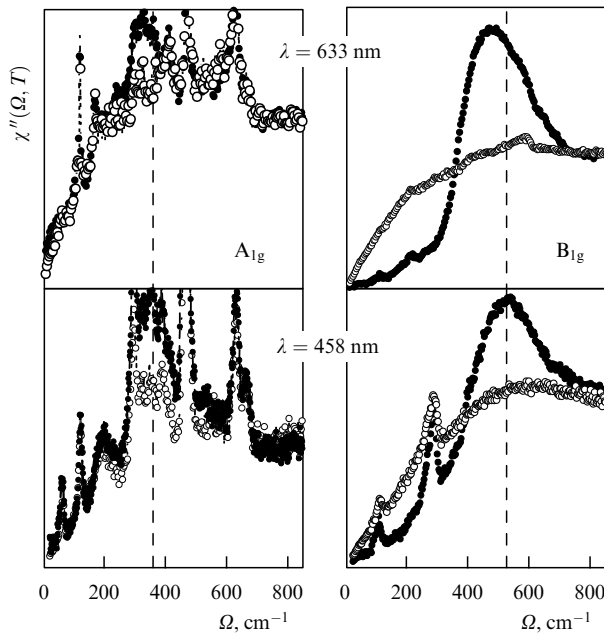


Figure 10. ERS spectra of A_{1g} - and B_{1g} -symmetries obtained through excitation by light of different wavelengths ($\lambda = 458$ nm and 633 nm) for the normal ($T = 100$ K, open circles) and superconducting ($T = 10$ K, full circles) states in optimally doped ($T_c = 91$ K) Bi2212. The vertical dashed lines help in visualizing the shift in the peak positions.

frequency range. To demonstrate these features, we examine the A_{1g} - and B_{1g} -spectra of the Bi2212 crystal at two different frequencies of exciting light (Fig. 10). By comparing the spectra we see that the positions of the ERS peaks and the low-frequency parts of the spectra in the superconducting state depend on the wavelength of the exciting light. The dependence $\Delta(\lambda)$ can be understood if we assume that the ERS matrix element depends on the wavelength of the exciting light, which is possible when the electron spectrum has a Van Hove singularity [94]. An alternative explanation is the dependence of the superconducting gap not only on the direction (angular dependence) in \mathbf{k} -space but also on the magnitude of the wave vector [119]. The latter becomes possible since, for HTSC the region in the \mathbf{k} -space in which the superconducting gap exists is large compared to the range of wave vectors accessible to ERS, i.e., the effect is caused by the smallness of the coherence length in HTSC's.

Owing to the fact that excitation of the ERS with light of $\lambda \geq 600$ nm makes it possible to avoid phonon excitation in the $x'y'$ -polarization spectra, a two-mode structure of the electron B_{1g} -symmetry peak was discovered for optimally doped Bi2212 single crystals [94]. Here one of the peak's components appears at a temperature somewhat above the superconducting transition temperature. A very similar temperature anomaly of the B_{1g} -peak was observed earlier for the lightly doped case and was associated with the existence of local pairs at temperatures $T < T^*$, where T^* is the temperature at which the pseudogap opens [118]. The two-mode structure of the peak in the case of optimal doping also suggests that there are electron pairs above T_c , which can be understood by using the ideas [123] that were proposed prior to the BCS ideology and are now being developed within the model of bipolaron superconductivity [124]. Based on observations of the two-mode structure of the peak and the peak's temperature dependence, there was an attempt to

describe superconductivity as the Bose condensation of quasiparticles [125] in the presence of a Van Hove singularity [94]. Here the researchers associated the emergence of the first peak above T_c with pair formation caused by the conversion of fermions into bosons for states near the singularity. These local electron pairs, responsible for the first peak, do not exhibit phase coherence which is realized only below T_c and leads to the emergence of the second peak caused by the appearance of off-diagonal long-range order (the coherence of the condensate). As the temperature decreases and the density of the superconducting condensate increases, the second peak begins to dominate and finally absorbs the first peak [94].

5.2 Light scattering with out-of-plane zz - and xz -polarizations

One of the features of HTSC's is the different nature of carrier motion in directions parallel and perpendicular to the CuO_2 planes. The very first investigations showed that in the metallic state the conductivity varies linearly with temperature for carriers that move parallel to the cuprate planes, while the conductivity along the c axis exhibits semiconductor behavior [126, 127]. The results of numerous experiments suggest that the mean free path of the carriers along the c axis is comparable to the lattice constant, i.e., normal transport is incoherent [127]. The reason is that one property inherent in all HTSC's is the fairly large crystalline anisotropy c/a (equal to 7.6 for Tl2212, 5.7 for Bi2212, and 3.0 for Y123). In the reciprocal space this anisotropy leads to an oblate Brillouin zone, which nevertheless possesses all the symmetry properties of the unit cell of a square or rectangular CuO_2 lattice. The results of band structure calculations suggest that all the energy bands relevant to the problem are related primarily to CuO_2 planes without substantial dispersion along the c axis [128–131]. Thus, band structure calculations and measurements of transport properties [127, 131–133] show that the effective carrier mass along the c axis is much larger than the in-plane mass, so that one could expect the ERS intensity in the zz -polarization to be negligible. However, experiments have shown that this is far from the case, even for superconductors with the greatest anisotropy, Tl2212 and Bi2212 [92, 121, 133, 134, 136]. The intensity of the electron component of the zz -spectrum is comparable to the intensity of in-plane polarizations [137, 138], which suggests a departure from the effective mass approximation and, apparently, indicates the need to account for resonance factors. The intensity of off-diagonal spectra is much lower, but nevertheless for some HTSC's these spectra have been recorded [139, 140].

As a result of transition to the superconducting state the out-of-plane electron continua become redistributed [98, 110, 121]. This is illustrated by Figs 11 and 12 which show the data for optimally doped Nd123 ($T_c = 95$ K) and Y123 ($T_c = 92$ K). The nature of the redistribution of the out-of-plane continua is qualitatively similar to the nature of the redistribution of in-plane polarization continua: suppression of scattering at low frequencies and the emergence of a broad peak caused by the breaking of Cooper pairs at high frequencies [98]. The very fact that the position of the E_g -component of the superconducting gap differs from the positions of the A_{1g} -, B_{1g} -, and B_{2g} -components observed in in-plane polarizations is natural and suggests that the superconducting order parameter in HTSC's is three-dimensional. However, it occurs that for the fully symmetrical components

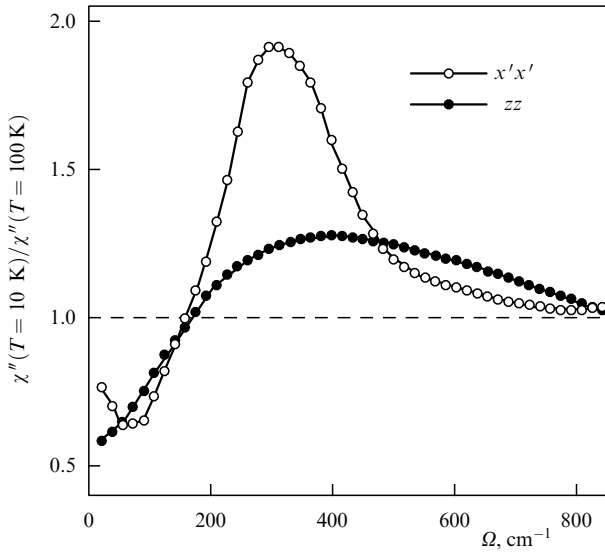


Figure 11. Ratio of ERS susceptibilities, χ''_s/χ''_n , for Nd123 obtained in the $x'x'$ -polarization ($A_{1g} + B_{2g}$ -symmetry, open circles) and in the zz -polarization (A_{1g} -symmetry, full circles).

of the ERS the positions of the 2Δ peak for the in-plane and out-of-plane polarizations also differ (see Fig. 11). Finding the positions of the 2Δ peak in the zz -polarization is

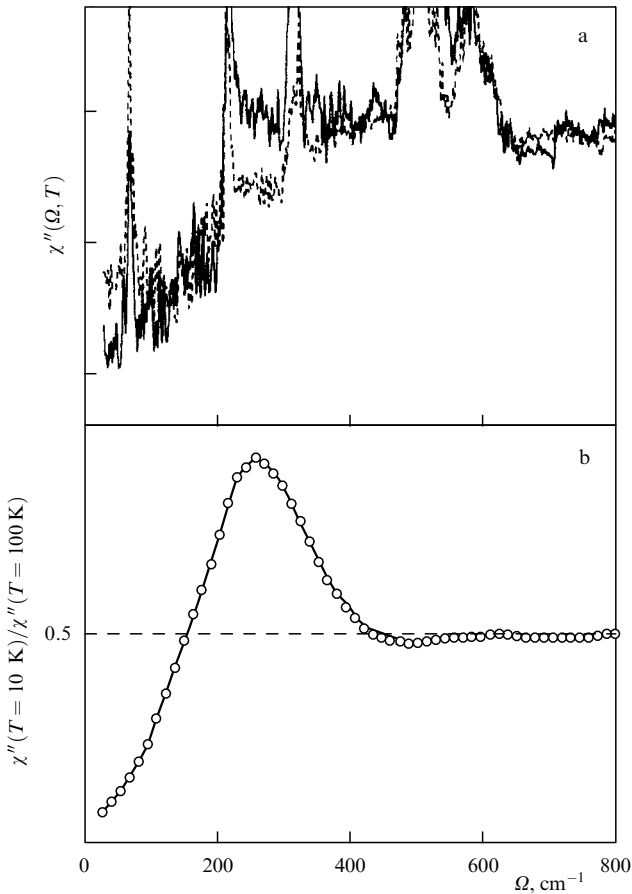


Figure 12. (a) ERS susceptibility in the zx -polarization for the normal ($T=100\text{ K}$, dashed curve) and superconducting ($T=10\text{ K}$, solid curve) states for the optimally doped ($T_c=92\text{ K}$) single crystal Y123, and (b) the ratio χ''_s/χ''_n .

complicated by the presence of strong phonon scattering which dominates in the spectrum. However, analysis of the χ''_s/χ''_n ratios for the in-plane and out-of-plane polarizations (shown in Fig. 11) suggests that $\Omega_{\max}(zz) > \Omega_{\max}(xx)$. Such behavior of the out-of-plane and in-plane electron continua in the superconducting state was also observed in optimally doped Bi2212 and Y123 [98, 133, 135]. The problem of the difference between out-of-plane and in-plane superconducting ERS spectra has yet to be resolved. This difference probably stems from the difference in the coherence lengths of the superconducting condensate and is related to the difference in lifetimes of the Cooper pairs for these two crystallographic directions. Such an assumption is corroborated by the fact that the 2Δ peak in the zz -polarization is broader than the 2Δ peak in the in-plane polarization, conclusive evidence of which is provided by the coincidence of the frequencies at which the normal and superconducting spectra intersect in the low-frequency region, $\Omega_1(s) = \Omega_1(n)$. An alternative explanation can be found in Ref. [133]. Noticing that two quasiparticles emerge in the final state of the Raman process, Kulić [133] assumed that in out-of-plane scattering these quasiparticles are created on different planes, while in in-plane scattering the quasiparticles are created on the same plane. Since these quasiparticles continue to interact, the interaction is responsible for renormalization of the gap. However, gap anisotropy is also observed in HTSC's with a single cuprate plane, which partially leaves Kulić's model [133] without experimental support. In addition, in one of the experiments the gap along the c axis was smaller than the in-plane gap, which was explained by the theory [135, 141].

5.3 Light scattering in HTSC's with different doping levels

ERS spectra of different symmetries differ even in the normal state. This anisotropy of the normal state was discovered in experiments practically at the same time as the discovery of the anisotropy of the superconducting state [142, 143], but has not received much attention from theoreticians who so far have mainly focused on phenomena below T_c . ERS in the normal state has been studied for Y123, La214, Bi2212, and Tl2212 [144–151]. Analysis has shown that for optimally doped HTSC crystals the intensity of the electron excitations of A_{1g} - and B_{1g} -symmetries in the normal state are comparable in value to and exceed the intensity of B_{2g} -symmetry excitations. This fact is illustrated by Fig. 13 which depicts the spectra of the main symmetries for optimally doped La214 at room temperature. In lightly doped superconductors, the intensity of normal B_{1g} -symmetry excitations drops and becomes lower than that of B_{2g} -symmetry excitations. In heavily doped HTSC's, the ERS appears to be fairly isotropic. This dependence of intensity on the doping level for different scattering channels is shown in Fig. 14 using the example of La124 [52]. The similarity of behavior of the scattering intensity of different symmetries depending on the doping level in such systems as La214, Y123, Bi2212, and Tl2212 serves as yet additional confirmation of the fact that scattering is due to the carriers of the CuO_2 planes and reflects the symmetry properties of these planes [24].

Changes in the doping level modify the ERS spectra in the superconducting state in a complicated way. For instance, when doping is light, the superconductivity-induced 2Δ peak of B_{1g} -symmetry gradually disappears [151] as the decrease in carrier concentration weakens the scattering in the normal

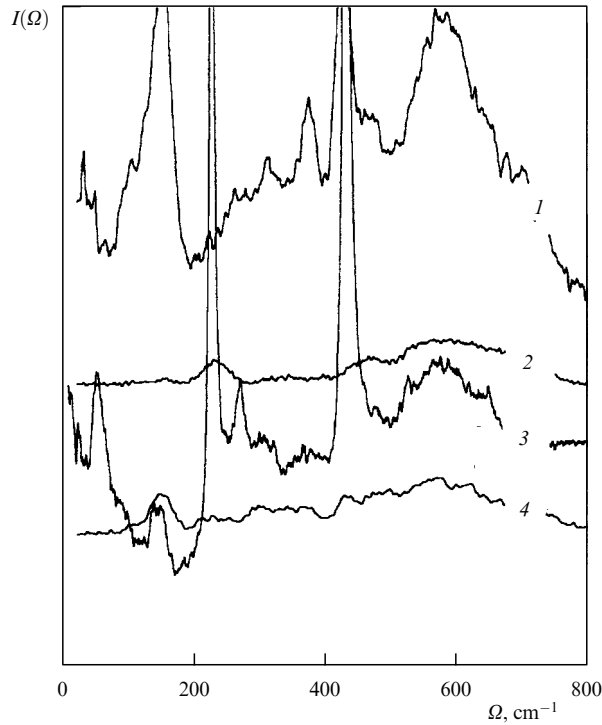


Figure 13. ERS spectra of different symmetries for the normal state ($T = 295$ K) of the optimally doped ($T_c = 34$ K) La214 single crystal: 1 — A_{1g} (xx), 2 — B_{1g} , 3 — A_{1g} (zz), and 4 — B_{2g} .

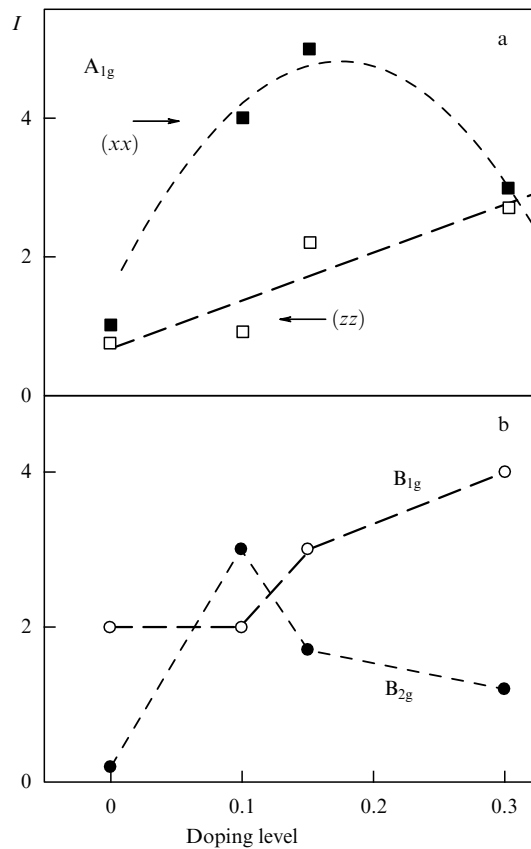


Figure 14. ERS intensity (measured at 800 cm^{-1}) of different symmetries in the normal state of La214 as a function of the doping level: (a) fully symmetrical components and (b) not fully symmetrical components.

state, while when doping is heavy, the frequencies of the ERS peaks of all symmetries practically coincide [146]. Doping leads to many complications, each of which may modify the ERS. Here are only some of these complications. First, oxygen vacancies and the substitution of metal ions may lead to a random potential capable of strongly scattering the electrons. Second, electron correlations are extremely sensitive to carrier concentration. Third, a decrease in carrier concentration in lightly doped samples leads to strong antiferromagnetic correlations. Up to now most of these complications have not received the proper attention of theoreticians studying the inelastic scattering of light in HTSC's.

As the carrier concentration becomes higher than the optimal value, the positions of the peaks of all symmetries are shifted to lower frequencies, with the shift of the B_{1g} -peak being the largest. This nonuniformity in the shift leads to a situation in which the peaks in the overdoped case appear practically at the same frequency, i.e., polarization anisotropy observed at optimal doping disappears [24]. The ratio $2\Delta/T_c$ for all symmetries is roughly equal to 6. Kendziora et al. [148] were the first to observe this in Bi2212, and this served as a basis for suggesting that s-symmetry pairing in overdoped HTSC's is predominant. However, here the low-frequency responses in the spectra remain polarization-dependent, and the cubic component is present in B_{1g} -symmetry spectra. Since low-frequency responses are less sensitive to the details of the band structure than the positions of the peaks, some researchers believe that d-symmetry is conserved at high doping levels, too [147, 149].

In lightly doped superconductors, superconductivity-induced changes are not detected in ERS spectra of A_{1g} - and B_{1g} -symmetries, and the only electron scattering channel which responds to superconductivity is still B_{2g} -symmetry scattering [24, 151]. Here the ratio $2\Delta/T_c$ remains practically unchanged and equal to 6.0. If we assume that the peaks of A_{1g} - and B_{1g} -symmetries stay at the same frequencies as in optimally doped crystals, this means that polarization anisotropy is much stronger in lightly doped HTSC's. This assumption is justified by the fact that up to now there have been no experimental indications that peaks of the A_{1g} - and B_{1g} -symmetries become less pronounced as the carrier concentration decreases. Rather, an analysis of the experimental data suggests that starting from a certain critical concentration (whose value has yet to be established) the peaks begin to fade away, staying approximately at the same frequencies as in optimally doped crystals. The upper limit of polarization anisotropy in underdoped crystals is specified by the value of the pseudogap and cannot exceed 4. A more realistic estimate, however, yields $\Omega_{B_{1g}}/\Omega_{B_{2g}} \approx 2$, which nevertheless is much higher than in optimally and heavily doped HTSC's. The study of gap excitations in underdoped superconductors is complicated by the fact that a pseudogap emerges in them at temperatures T^* much higher than T_c , with the pseudogap manifesting itself as suppression of scattering in the frequency range extending from zero to $700\text{--}800\text{ cm}^{-1}$. This situation is illustrated by Fig. 15, which depicts two spectra for Y123 at temperatures below T_c . Since the strongest suppression of scattering is observed in xy -polarization spectra, we can assume that the pseudogap is preferably B_{2g} -symmetric, thus contradicting the interpretation of photoemission data, which assigns to the pseudogap the same symmetry as that of the superconducting gap [24]. However, this contradiction can be resolved if we take into

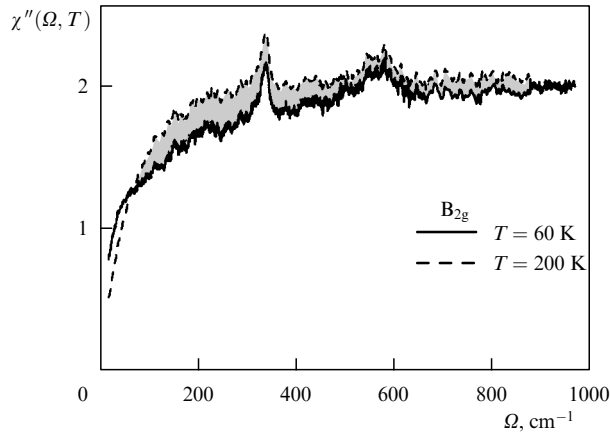


Figure 15. Manifestation of the pseudogap in B_{2g} -symmetry spectra of lightly doped Y123 ($T_c = 57$ K). The solid curve corresponds to the spectrum at $T = 60$ K, the dashed curve corresponds to the spectrum at $T = 200$ K, and the hatched region shows the loss of spectral weight.

account that as the carriers are expelled from the system the shape of the Fermi surface changes. Figure 16 shows the two gaps for the two limiting cases of doping. In lightly doped HTSC's, the amplitude of the d-type pseudogap exceeds that of the superconducting gap of the same symmetry. Hence the superconducting gap is well-defined only near those sections of the Fermi surface that are probed by the B_{2g} -symmetry channel. The reason is that the pseudogap and the superconducting gap differ in shape (but not in symmetry!). As the number of carriers increases, the area of the Fermi surface and the superconducting gap increase, which leads to a situation in which the different scattering channels 'see' the superconducting gap in different sections of the Fermi surface.

By now the absence of phase coherence in pseudogap formation has firmly been established by the ERS methods [24, 147, 153], thus setting the pseudogap well apart from the superconducting gap for which phase coherence, ensured by the specific character of BCS pairing, follows from many experiments, including those involving inelastic light scattering. Nevertheless, we can hope that the presence of a pseudogap will help to explain a number of anomalies in ERS in the superconducting state, especially the temperature dependence of the positions of ERS peaks. There is no generally accepted explanation of pseudogap formation,

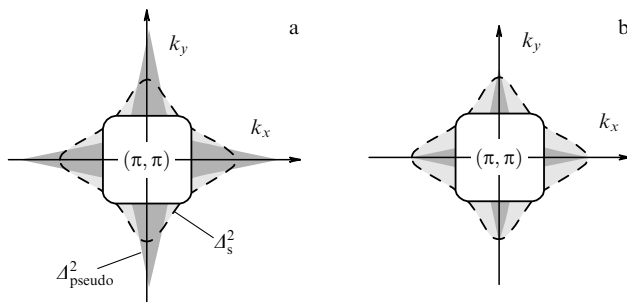


Figure 16. Schematic representation of the pseudogap Δ_{pseudo} and the superconducting gap Δ_s for lightly (a) and optimally (b) doped superconductors. The hatched area corresponds to the pseudogap and the dashed curve represents the superconducting gap.

although some possible mechanisms are discussed in Refs [152–154].

Since at all doping levels the ratio $2\Delta/T_c$ is no smaller than 6, we can assume that irrespective of the doping level high- T_c superconductivity is realized in the strong-coupling limit. Interestingly, the only scattering channel in which the position of the ERS peak 'tracks' the superconducting transition temperature is B_{2g} -symmetry scattering. In the other two symmetries, A_{1g} and B_{1g} , there is no proportionality between the position of the low-temperature ERS peak and T_c .

5.4 Van Hove singularity and inelastic light scattering

The singularity in the density of electronic states near the Fermi level has attracted much attention as a possible reason for the high transition temperature and the remarkable properties of the normal state of HTSC's [155]. Experimental photoemission data have presented a direct proof of the existence of an extended Van Hove singularity in some regions of the Brillouin zone [22]. In these regions, the dispersion law for the carriers is highly anisotropic and can be represented in the form of a saddle elongated along the y axis:

$$\varepsilon(\mathbf{k}) = \frac{1}{2} \left(\frac{k_x^2}{m} - \frac{k_y^2}{M} \right) - E_0.$$

The typical value of E_0 is about $200\text{--}250\text{ cm}^{-1}$ and, since inelastic light scattering is the indirect interaction of light and low-energy crystal excitations, it is sensitive to the details of the band structure and may manifest itself in ERS spectra. Indeed, the experimental data on ERS for compounds $\text{YBa}_2\text{Cu}_3\text{O}_{7-x}$ with different values of x , $\text{YBa}_2\text{Cu}_4\text{O}_8$, $\text{Bi}_2\text{Sr}_2\text{CaCu}_2\text{O}_{8+x}$, $\text{Bi}_2\text{Sr}_2\text{CuO}_{6+x}$, and $\text{Tl}_2\text{Ba}_2\text{CuO}_{6+x}$ indicate that the fully symmetrical spectra of these compounds contain a broad line at $\Omega \approx 200\text{ cm}^{-1}$ whose intensity increases with decreasing temperature [25, 116]. These lines are absent in the B_{1g} - and B_{2g} -spectra of superconducting crystals and in all symmetries of scattering in nonsuperconducting crystals. This body of experimental data makes it possible to tentatively assign the given line to the extended Van Hove singularity. A possible scattering mechanism for this case is the excitation of electron–hole pairs with a large quasimomentum, whose production is due to the fact that near the singularity the carriers move more slowly and their damping is much smaller than in the case far from the singularity [156, 157]. As noted in Section 3, examining the scattering in the broad frequency range characteristic of HTSC's requires employing different mechanisms of momentum relaxation. These mechanisms may manifest themselves in two interdependent ways. First, momentum relaxation leads to a finite damping of the excitations with exceptionally small momentum $q \approx 1/\delta$, i.e., to their finite spectral density within a frequency range whose width is of the order $1/\tau_r$, where τ_r is the characteristic relaxation time. Second, the finite value of τ_r allows the appearance in Raman scattering of excitations with high values of momentum, $q \gg 1/\delta$. It is only natural to assume that $\tau_r \leq 1/E_0$, i.e., $\tau_r \leq 3 \times 10^{-14}\text{ s}$. The corresponding mean free path $l = v_F \tau_r \approx 1.5\text{ nm}$, and, in view of the uncertainty of the wave vector, the possible momentum transfer to the electron subsystem is determined by the mean free path rather than by the light penetration depth, i.e., $q_1 \approx 1/l \gg q_\delta$. The mechanism allows scattering within the range of frequencies of the order $v_F q_1$, which may be much larger than E_0 . In the given process, an electron

excited by light creates an electron–hole pair with momentum \mathbf{q} , due to the interaction with other electrons. Since the momentum of the scattered photon practically coincides with that of the exciting photon, to balance the momentum of the electron–hole pair a momentum $-\mathbf{q}$ must be transferred to the crystal because of phonon excitation and/or scattering by an impurity. Hence the given process is determined by both electron–electron interaction and the quasimomentum relaxation rate. The corresponding intensity $I(\Omega)$ is proportional to $V^2\tau^{-1}$, where V is the matrix element of carrier interaction, $\tau = \min\{\tau_i, \tau_{e-ph}\}$, with τ_{e-ph} and τ_i the relaxation times determined by the electron–phonon interaction and the impurity scattering, respectively. This intensity can be estimated as

$$I(\Omega) \propto V^2\tau^{-1} \int_{-E_0}^0 v(\varepsilon)v(\varepsilon + \Omega) d\varepsilon,$$

where $\varepsilon < 0$ (occupied states), and $\varepsilon + \Omega > 0$ (vacant states). For $\Omega < E_0$, the small phase volume of possible excitations leads to a small scattering intensity. For $\Omega > E_0$, the density of states decreases, which leads to a decrease in the scattering intensity. This implies that the intensity has a maximum at a frequency Ω determined by the singularity energy E_0 . When pairs with a finite momentum are generated, the carriers are redistributed in \mathbf{k} -space, and the presence of a Van Hove singularity assists redistribution. To experimentally verify the above mechanism of the manifestation of a Van Hove singularity in ERS spectra, one must first prove the electron nature of the peak that emerges at 200 cm^{-1} . Although many properties of the peak point to this [25, 116, 151, 157], the proximity of the peak's energy to the characteristic phonon energies requires the possibility of such a peak emerging because of disorder-induced scattering by IR phonons to be excluded. To do this we must identify the phonon mode that could manifest itself in Raman scattering spectra, perform an isotopic substitution of the atom dominating in the normal vector of the phonon, and observe the respective isotopic shift of the frequency of this mode.

Note that the effect of a Van Hove singularity on inelastic light scattering is not only a direct manifestation in the spectra. The presence of a singularity modifies the screening, violates the requirements of the Migdal theorem, and, as a result, requires a thorough review of the simplified theories of inelastic scattering, which do not allow for peculiarities of the electron spectrum [25]. The effect of a Van Hove singularity on the ERS matrix element was studied by Sherman [157] and Branch and Carbotte [158]. They found that although the anisotropy of the ERS matrix element is larger than the anisotropy of the Fermi surface, it is still much smaller than the anisotropy of the effective mass tensor. From this it follows that the contribution of states near the maxima and minima of the superconducting gap in a superconductor with a d-type gap is determined by a large number of harmonics of the Brillouin zone. The anisotropy of the ERS matrix element may play a substantial role in fully symmetrical scattering. Since the expansion of the fully symmetrical matrix element contains a large number of Fermi-surface harmonics $\varphi_L(\mathbf{k})$, it may occur that the fundamental harmonic ($L = 0$) is screened by the Coulomb interaction, but the higher-order harmonics ($L = 2, 4, 6, \dots$) are not, and it is these higher harmonics that are responsible for the anomalous intensity of the fully symmetrical component [158.]

6. Symmetry of the order parameter, pairing, and possible superconductivity mechanisms

Thus, by studying the polarization, temperature, and resonance dependences of ERS in the superconducting state and the role that doping and impurities play in the emergence of superconductivity-induced changes, it is possible to determine the most probable symmetry of the order parameter. When doping is optimal, the superconducting gap is anisotropic and has zeros on the Fermi surface. Here it is almost common knowledge that the B_{1g} -component of the symmetry of the order parameter dominates. Nevertheless, the zeros of the order parameter are either shifted from the positions on the diagonals of the Brillouin zone or exist within a finite region near the diagonals. Such a topology of the zeros may indicate that there is an admixture of the A_{1g} -component, which may appear because of orthorhombic distortions that transform the B_{1g} - and A_{1g} -components into the same irreducible representation A_g of group D_{2h} . This is possible in the compound Y123 in which the transition to the orthorhombic system is accompanied by the loss of such symmetry elements as the axis C_4 and the mirror plane σ_v . In Bi2212 the nature of the orthorhombic distortions is such that the mirror planes remain as symmetry elements, so that the B_{1g} - and A_{1g} -components belong to different irreducible representations. However, in both cases the integral of the order parameter over the Fermi surface is likely to be nonzero. This points to a multicomponent (most likely $d + s$) order parameter when the doping of HTSC is optimal since, on the basis of general symmetry considerations, in the case of orthorhombic lattice it is impossible to avoid mixing of the s - and d -components of the order parameter [159, 160]. One cannot exclude the possibility that the pairing symmetry is more exotic; this possibility was studied in detail by Krantz [90]. It must be noted, however, that pure g -pairing cannot produce the maxima in the order parameter along the principal axes of the Brillouin zone, while mixed states of the $g + id$ type lead to spontaneous breaking of time-reversal symmetry, which has not yet been irrevocably proved by experiments [161].

The anisotropy of the order parameter decreases as doping grows, but the zeros do not disappear for the highest carrier concentrations realized so far. This is implied by the absence of scattering thresholds and is probably due to the fact that pairing symmetry remains unchanged irrespective of the doping level.

As the carrier concentration decreases, two of the three ERS components cease to respond to the transition to the superconducting state. The polarization that signalizes the phase transition is the one that probes the Brillouin-zone diagonals and B_{2g} -symmetry excitations. Here for the given polarization the ratio $2\Delta/T_c \approx 6.0$, as for optimal and heavy doping.

Observation of the preferential d -symmetry of the order parameter at optimal doping agrees with the results obtained by other spectroscopic and phase-sensitive methods [15, 21, 22]. However, as the doping level changes, there still exist unexplained differences in the behavior of the superconducting gap observed through different experimental methods [24]. The problem of how universal and stable the $d_{x^2-y^2}$ -symmetry is has yet to find its solution. On the basis of the existing experimental ERS data we can assume that the contribution of the d -channel of pairing decreases when the carrier concentration deviates from the optimal

value. Speaking in favor of this assumption is the large number of theoretical papers that point out that the stability of the $d_{x^2-y^2}$ -symmetry order parameter depends on the details of the band structure and the pairing potential [162, 163]. In the presence of two pairing channels, the pairing symmetry depends on electron band filling and the band parameters. Here the d-symmetry is predominant at half-band filling, while s-symmetry is more stable in cases of light and heavy doping [163–166].

The fact that d-symmetry pairing is predominant is frequently considered as an indication that phonons do not provide the main contribution to the formation of the superconducting state. Indeed, d-symmetry pairing was introduced in order to explain high- T_c superconductivity that occurs via the exchange of antiferromagnetic spin fluctuations [167, 168]. How phonons and electron–phonon interaction contribute to the formation of a high T_c is not obvious and is still a topic of discussion [132, 169]. However, in recent years a large number of theoretical papers that point to the importance of electron–phonon interaction in realizing high transition temperatures, even for the d-pairing case, has appeared [163]. There is also a large body of experimental evidence, partially obtained by the Raman scattering, of the reaction of the HTSC lattice to the transition to the superconducting state [170, 171]. Here it will suffice to remind that the electron continuum whose redistribution determines the pairing symmetry, emerges largely because of strong electron–phonon interaction [70]. The last, but not least in significance, example of the importance of the electron–phonon interaction in the formation of a high superconducting-transition temperature is the recent discovery of superconductivity in the intermetallic compound MgB_2 with $T_c = 39$ K [172].

7. Conclusions

The detailed experimental investigations of the superconducting state in various classes of HTSC's show that the ERS is an indispensable, and often unique, method for establishing the anisotropy and symmetry of the order parameter. The power of this method stems from the capability of ERS to probe various regions of the Fermi surface by simply varying the polarizations of the exciting and scattered light, which makes it possible to monitor the changes in the order parameter in different areas of the momentum space and to compensate for the absence of true resolution in the wave vector. Although the resolution in \mathbf{k} in ERS cannot be compared to that achieved by photoemission, it nevertheless is better than the resolutions inherent in many methods that measure various correlation functions averaged over the entire Fermi surface (infrared and tunnel spectroscopies, calorimetry, etc.). Moreover, the ERS is sensitive to coherence factors, while other spectroscopic methods usually respond to any gap in the density of states.

The methods of inelastic light scattering have reliably established that the superconducting gap in HTSC's is anisotropic and has zeros in separate regions of the Fermi surface. Anisotropy decreases as the doping increases, but the zeros do not disappear at the highest carrier concentrations realized so far. The bismuth, yttrium–barium, mercury, and lanthanum systems belong to the most thoroughly studied group of superconductors. Most ERS experiments attest to the preferential nature of d-symmetry pairing (at least at optimal doping), although the admixture of the s-component

may be substantial, especially for compounds of the yttrium–barium group. Among the unresolved problems that require the combined effort of experimenters and theoreticians are those of resonance properties, the contribution of A_{2g} -symmetry scattering, and inclusion of the coherence properties of the initial state into the theoretical description of the process.

In conclusion, I would like to express my gratitude to my colleagues for the numerous discussions and the help they provided. I am especially grateful to E Ya Sherman for the many years of collaboration that determined the content of this review, and to E G Maksimov for fruitful discussions. This work was made possible by the financial support of the Russian Foundation for Basic Research (Grant 01-02-16480a) and the Alexander von Humboldt Foundation (Germany).

References

1. Bednorz J G, Müller K A Z. *Phys. B: Cond. Mat.* **64** 189 (1986)
2. Ginzburg V L, Landau L D *Zh. Eksp. Teor. Fiz.* **20** 1064 (1950) [L D Landau *Collected Papers* (London: Pergamon Press, 1965) p. 546]
3. Gor'kov L P *Zh. Eksp. Teor. Fiz.* **36** 1918; **37** 1407 (1959) [*Sov. Phys. JETP* **9** 1364 (1959); **10** 1063 (1960)]
4. Cooper L N *Phys. Rev.* **104** 1189 (1956)
5. Bardeen J, Cooper L N, Schrieffer J R *Phys. Rev.* **108** 1175 (1957)
6. Gough C E et al. *Nature* **326** 855 (1987)
7. Abrikosov A A, Fal'kovskii L A *Zh. Eksp. Teor. Fiz.* **40** 262 (1961) [*Sov. Phys. JETP* **13** 179 (1961)]
8. Devereaux T P et al. *Phys. Rev. Lett.* **72** 3291 (1994)
9. Yang C N *Rev. Mod. Phys.* **34** 694 (1962)
10. Lifshitz E M, Pitaevskii L P *Statisticheskaya Fizika* (Statistical Physics) Pt. 2 *Teoriya Kondensirovannogo Sostoyaniya* (Theory of Condensed Matter) (Moscow: Fizmatlit, 1978) [Translated into English (Oxford: Pergamon Press, 1980)]
11. Landau L D *Zh. Eksp. Teor. Fiz.* **7** 19 (1937)
12. Anderson P W *Phys. Rev.* **112** 1900 (1958)
13. Volovik G E, Gor'kov L P *Zh. Eksp. Teor. Fiz.* **88** 1412 (1985) [*Sov. Phys. JETP* **61** 843 (1985)]
14. Pals J A, van Haeringen W, van Maaren M H *Phys. Rev. B* **15** 2592 (1977)
15. Tsuei C C, Kirtley J R *Rev. Mod. Phys.* **72** 969 (2000)
16. Landau L D, Lifshitz E M *Statisticheskaya Fizika* (Statistical Physics) Pt. 1 (Moscow: Fizmatlit, 1995) [Translated into English (Oxford: Pergamon Press, 1980)]
17. Shaked H et al. *Crystal Structures of the High- T_c Superconducting Copper-Oxides* (Amsterdam: Elsevier, 1994)
18. Sigrist M, Rice T M *Rev. Mod. Phys.* **67** 503 (1995)
19. Schrieffer J R *Solid State Commun.* **92** 129 (1994)
20. Lu J P *Phys. Rev. Lett.* **68** 125 (1992)
21. Norman M R et al. *Phys. Rev. B* **52** 615 (1995)
22. Shen Z-X, Dessau D S *Phys. Rep.* **253** 1 (1995)
23. Becherer Th et al. *Int. J. Mod. Phys. B* **7** 123 (1993)
24. Hackl R, in *The Gap Symmetry and Fluctuations in High- T_c Superconductors* (NATO ASI Series, Ser. B, Vol. 371, Eds J Bok et al.) (New York: Plenum Press, 1998) p. 249
25. Sherman E Ya, Misochko O V, Lemmüns P, in *Spectroscopy of High- T_c Superconductors: A Theoretical View* (Ed. N M Plakida) (London: Taylor & Francis Books Ltd, 2002) p. 97
26. Feile R *Physica C* **159** 1 (1989)
27. Thomsen C, in *Light Scattering in Solids VI: Recent Results, Including High- T_c Superconductivity* (Topics in Applied Physics, Vol. 68, Eds M Cardona, G Güntherodt) (Berlin: Springer-Verlag, 1991) p. 285
28. Cardona M *Physica C* **317–318** 30 (1999)
29. Abrikosov A A, Falkovsky L A *Physica C* **156** 1 (1988)
30. Devereaux T P, Einzel D *Phys. Rev. B* **51** 16336 (1995)
31. Verkin B I, Lazarev B G *Izv. Akad. Nauk SSSR. Ser. Fiz.* **12** 598 (1948)

32. Khaikin M S, Bykov V P *Zh. Eksp. Teor. Fiz.* **30** 191 (1956) [*Sov. Phys. JETP* **3** 119 (1956)]
33. Abrikosov A A, Genkin V M *Zh. Eksp. Teor. Fiz.* **65** 842 (1973) [*Sov. Phys. JETP* **38** 417 (1974)]
34. Fraas L M, Williams P F, Porto S P S *Solid State Commun.* **8** 2113 (1970)
35. Sooryakumar R, Klein M V *Phys. Rev. Lett.* **45** 660 (1980)
36. Sooryakumar R, Klein M V *Phys. Rev. B* **23** 3213 (1981)
37. Hackl R, Kaiser R, Schicktanz S J. *Phys. C: Solid State Phys.* **16** 1729 (1983)
38. Dierker S B et al. *Phys. Rev. Lett.* **50** 853 (1983)
39. Klein M V, Dierker S B *Phys. Rev. B* **29** 4976 (1984)
40. Bazhenov A V et al. *Pis'ma Zh. Eksp. Teor. Fiz.* **46** (Supplement) 35 (1987) [*JETP Lett.* **46** (S1) S29 (1987)]
41. Lyons K B et al. *Phys. Rev. B* **36** 5592 (1987)
42. Fal'kovskii L A *Zh. Eksp. Teor. Fiz.* **95** 1146 (1989) [*Sov. Phys. JETP* **68** 661 (1989)]
43. Yamanaka A et al. *Jpn. J. Appl. Phys. Pt. 2* **27** L1902 (1988)
44. Nemetschek R et al. *Phys. Rev. B* **47** 3450 (1993)
45. Maksimov A A, Tartakovskii I I, Timofeev V B *Pis'ma Zh. Eksp. Teor. Fiz.* **50** 44 (1989) [*JETP Lett.* **50** 51 (1989)]
46. Krantz M C et al. *Phys. Rev. B* **40** 2635 (1989)
47. Hackl R et al. *Phys. Rev. B* **38** 7133 (1988)
48. Cooper S L et al. *Phys. Rev. B* **37** 5920 (1988)
49. Staufer T et al. *Phys. Rev. Lett.* **68** 1069 (1992)
50. Chen X K et al. *Phys. Rev. Lett.* **73** 3290 (1994)
51. Chen X K et al. *Physica C* **295** 80 (1998)
52. Misochko O V, Uchida S *Phys. Lett. A* **248** 423 (1998)
53. Heyen E T et al. *Phys. Rev. B* **43** 12958 (1991)
54. Donovan S et al. *J. Supercond.* **8** 417 (1995)
55. Sacuto A et al. *Phys. Rev. B* **58** 11721 (1998)
56. Sacuto A et al. *Phys. Rev. B* **61** 7122 (2000)
57. Hadjiev V G et al. *Phys. Rev. B* **58** 1043 (1998)
58. Stadlober B et al. *Phys. Rev. Lett.* **74** 4911 (1995)
59. Blumberg G et al. *Phys. Rev. Lett.* **88** 107002 (2002)
60. Els G et al. *Physica C* **307** 79 (1998)
61. Chen X K et al. *Phys. Rev. Lett.* **87** 157002 (2001)
62. Quilty J W et al. *Phys. Rev. Lett.* **88** 087001 (2002)
63. Madelung O *Festkörpertheorie I, II* (Berlin: Springer-Verlag, 1972) [Translated into English: *Introduction to Solid-State Theory* (Berlin: Springer-Verlag, 1978) [Translated into Russian (Moscow: Nauka, 1980)]
64. Sushchinskii M M *Spektry Kombinatsionnogo Rasseyaniya Molekul i Kristallov* (Raman Spectra of Molecules and Crystals) (Moscow: Nauka, 1969) [Translated into English (New York: Wiley, 1972)]
65. Kosztin J, Zawadowski A *Solid State Commun.* **78** 1029 (1991)
66. Wolff P A *Phys. Rev.* **171** 436 (1968)
67. Zawadowski A, Cardona M *Phys. Rev. B* **42** 10732 (1990)
68. Shastry B S, Shraiman B I *Phys. Rev. Lett.* **65** 1068 (1990)
69. Quinlan S M, Hirschfeld P J, Scalapino D J *Phys. Rev. B* **53** 8575 (1996)
70. Kostur V N, Éliashberg G M *Pis'ma Zh. Eksp. Teor. Fiz.* **53** 373 (1991) [*JETP Lett.* **53** 391 (1991)]
71. Kostur V N Z. *Phys. B: Cond. Mat.* **89** 149 (1992)
72. Strohm T, Cardona M *Phys. Rev. B* **55** 12725 (1997)
73. Varma C M et al. *Phys. Rev. Lett.* **63** 1996 (1989); Erratum *Phys. Rev. Lett.* **64** 497 (1990)
74. Tsuneto T *Phys. Rev.* **118** 1029 (1960)
75. Krantz M C, Cardona M *Phys. Rev. Lett.* **72** 3290 (1994)
76. Misochko O V *Int. J. Mod. Phys. B* **14** 1501 (2000)
77. Maksimov A A et al. *Solid State Commun.* **81** 407 (1992)
78. Bock A *Phys. Rev. B* **51** 15506 (1995)
79. Sugai S, Sato M *Phys. Rev. B* **40** 9292 (1989)
80. Staufer T, Hackl R, Müller P *Solid State Commun.* **79** 409 (1991)
81. Salamon D et al. *Phys. Rev. B* **51** 6617 (1995)
82. Manske D et al. *Phys. Rev. B* **56** R2940 (1997)
83. Venturini F et al. *Phys. Rev. B* **62** 15204 (2000)
84. Chubukov A V, Morr D K, Blumberg G *Solid State Commun.* **112** 183 (1999)
85. Strohm T, Munzar D, Cardona M *Phys. Rev. B* **58** 8839 (1998)
86. Tokura Y, Takagi H, Uchida S *Nature* **337** 345 (1989)
87. Sacuto A, Balkanski M, Gorochoy O *Solid State Commun.* **85** 589 (1993)
88. Thomsen C et al. *Phys. Rev. B* **37** 9860 (1988)
89. Slakey F et al. *Phys. Rev. B* **39** 2781 (1989)
90. Krantz M *Phys. Rev. B* **54** 1334 (1996)
91. Misochko O V *Zh. Eksp. Teor. Fiz.* **121** 406 (2002) [*JETP* **94** 345 (2002)]
92. Gu G, Misochko O V *Physica C* **288** 115 (1997)
93. Sherman E Ya, Ambrosch-Draxl C, Misochko O V *Phys. Rev. B* **65** 140510(R) (2002)
94. Misochko O V, Sherman E Ya *J. Phys.: Condens. Matter.* **12** 9095 (2000)
95. Stadlober B et al. *Physica B* **194–196** 1539 (1994)
96. Krantz M C, Cardona M J. *Low Temp. Phys.* **99** 205 (1995)
97. Strohm T, Cardona M *Solid State Commun.* **104** 233 (1997)
98. Misochko O V, Kuroda K, Koshizuka N *Phys. Rev. B* **56** 9116 (1997)
99. Misochko O V *Solid State Commun.* **113** 141 (1999)
100. Izyumov Yu A *Usp. Fiz. Nauk* **169** 225 (1999) [*Phys. Usp.* **42** 215 (1999)]
101. Gor'kov L P, Kalugin P A *Pis'ma Zh. Eksp. Teor. Fiz.* **41** 208 (1985) [*JETP Lett.* **41** 253 (1985)]
102. Borkowski L S, Hirschfeld P J *Phys. Rev. B* **49** 15404 (1994)
103. Fehrenbacher R, Norman M R *Phys. Rev. B* **50** 3495 (1994)
104. Lee P A *Phys. Rev. Lett.* **71** 1887 (1993)
105. Basov D N et al. *Phys. Rev. B* **49** 12165 (1994)
106. Hirschfeld P J, Putikka W O, Scalapino D J *Phys. Rev. B* **50** 10250 (1994)
107. Devereaux T P *Phys. Rev. Lett.* **74** 4313 (1995)
108. Devereaux T P, Kampf A P *Int. J. Mod. Phys. B* **11** 2093 (1997)
109. Wu W C, Carbotte J P *Phys. Rev. B* **57** R5614 (1998)
110. Misochko O V, Gu G *Phys. Rev. B* **59** 11183 (1999)
111. Misochko O V et al. *Phys. Rev. B* **60** 1326 (1999)
112. Devereaux T P J. *Supercond.* **8** 421 (1995)
113. Pokrovsky S V, Pokrovsky V L *Phys. Rev. Lett.* **75** 1150 (1995)
114. Mao W, Balatsky A V *Phys. Rev. B* **59** 6024 (1999)
115. Yamanaka A et al. *Phys. Rev. B* **46** 516 (1992)
116. Misochko O V, Sherman E Ya *Int. J. Mod. Phys. B* **12** 2455 (1998)
117. Misochko O V, Arslanbekov A Kh *Mod. Phys. Lett. B* **6** 1137 (1992)
118. Blumberg G et al. *Science* **278** 1427 (1997)
119. Misochko O V *Fiz. Tverd. Tela* **40** 998 (1998) [*Phys. Solid State* **40** 914 (1998)]
120. Klein M, in *Light Scattering in Solids II: Basic Concepts and Instrumentation* (Topics in Applied Physics, Vol. 50, Eds M Cardona, G Güntherodt) (Berlin: Springer, 1982) p. 148
121. Kang M et al. *Phys. Rev. Lett.* **77** 4434 (1996)
122. Rashkeev S N, Wendin G *Phys. Rev. B* **47** 11603 (1993)
123. Schafroth M R *Phys. Rev.* **100** 463 (1955)
124. Alexandrov A S, Mott N F *Polarons & Bipolarons* (Singapore: World Scientific, 1995)
125. Geshkenbein V B, Ioffe L B, Larkin A I *Phys. Rev. B* **55** 3173 (1997)
126. Cooper S L, Gray K E, in *Physical Properties of High Temperature Superconductors IV* (Ed. D M Ginsberg) (Singapore: World Scientific, 1994) p. 61
127. Ito T et al. *Nature* **350** 596 (1991)
128. Krakauer H, Pickett W E, Cohen R E J. *Supercond.* **1** 111 (1988)
129. Krakauer H, Pickett W E *Phys. Rev. Lett.* **60** 1665 (1988)
130. Hamann D R, Mattheiss L F *Phys. Rev. B* **38** 5138 (1988)
131. Shulga S V, Dolgov O V, Maksimov E G *Physica C* **178** 266 (1991)
132. Maksimov E G *Usp. Fiz. Nauk* **170** 1033 (2000) [*Phys. Usp.* **43** 965 (2000)]
133. Kulić M L *Phys. Rep.* **338** 1 (2000)
134. Gasparov L V et al. *Zh. Eksp. Teor. Fiz.* **96** 2115 (1989) [*Sov. Phys. JETP* **69** 1196 (1989)]
135. Boekholt M, Hoffmann M, Güntherodt G *Physica C* **175** 127 (1991)
136. Liu H L et al. *Phys. Rev. Lett.* **82** 3524 (1999)
137. McCarty K F et al. *Phys. Rev. B* **42** 9973 (1990)
138. McCarty K F et al. *Phys. Rev. B* **43** 13751 (1991)
139. Timofeev V B et al. *Physica C* **162–164** 1409 (1989)
140. Maksimov A A et al. *Phys. Rev. B* **54** R6901 (1996)
141. Abrikosov A A *Physica C* **182** 191 (1991)
142. Slakey F et al. *Phys. Rev. B* **43** 3764 (1991)
143. Sugai S et al. *Solid State Commun.* **76** 365 (1990)
144. Katsufuji T et al. *Phys. Rev. B* **48** 16131 (1993)
145. Chen X K et al. *Phys. Rev. B* **56** R513 (1997)

146. Kendziora C, Rosenberg A *Phys. Rev. B* **52** R9867 (1995)
147. Opel M et al. *Phys. Rev. B* **61** 9752 (2000)
148. Kendziora C, Kelley R J, Onellion M *Phys. Rev. Lett.* **77** 727 (1996)
149. Naeini J G et al. *Phys. Rev. B* **59** 9642 (1999)
150. Chen X K et al. *Phys. Rev. B* **56** R513 (1997)
151. Zaitsev S V et al. *Pis'ma Zh. Eksp. Teor. Fiz.* **61** 842 (1995) [*JETP Lett.* **61** 865 (1995)]
152. Timusk T, Statt B *Rep. Prog. Phys.* **62** 61 (1999)
153. Sadovskii M V *Usp. Fiz. Nauk* **171** 539 (2001) [*Phys. Usp.* **44** 515 (2001)]
154. Nemetschek R et al. *Phys. Rev. Lett.* **78** 4837 (1997)
155. Markiewicz R S J. *Phys. Chem. Solids* **58** 1179 (1997)
156. Misochko O V, Sherman E Ya *Physica C* **222** 219 (1994)
157. Sherman E Ya *Phys. Rev. B* **58** 14187 (1998)
158. Branch D, Carbotte J P *Phys. Rev. B* **54** 13288 (1996)
159. Walker M B, Luettmer-Strathmann J *Phys. Rev. B* **54** 588 (1996)
160. Béal-Monod M T *Phys. Rev. B* **58** 8830 (1998)
161. Sigrist M *Prog. Theor. Phys.* **99** 899 (1998)
162. Dagotto E *Rev. Mod. Phys.* **66** 763 (1994)
163. Varelogiannis G *Solid State Commun.* **107** 427 (1998)
164. Wheatley J, Xiang T *Solid State Commun.* **88** 593 (1993)
165. Koltenbah B E C, Joynt R *Rep. Prog. Phys.* **60** 23 (1997)
166. Carbotte J P, O'Donovan C *Physica C* **252** 87 (1995)
167. Miyake K, Schmitt-Rink S, Varma C M *Phys. Rev. B* **34** 6554 (1986)
168. Scalapino D J, Loh E (Jr), Hirsch J E *Phys. Rev. B* **34** 8190 (1986)
169. Ginzburg V L *Usp. Fiz. Nauk* **167** 429 (1997) [*Phys. Usp.* **40** 407 (1997)]
170. Hadjiev V G et al. *Phys. Rev. B* **58** 1043 (1998)
171. Misochko O V et al. *Phys. Rev. B* **59** 11495 (1999)
172. Nagamatsu J et al. *Nature* **410** 63 (2001)